

## Research paper

# Geochemical characteristics, redox conditions, and organic matter accumulation of marine oil shale from the Changliang Mountain area, northern Tibet, China



Shengqiang Zeng <sup>a, b</sup>, Jian Wang <sup>a, b, \*</sup>, Xiugen Fu <sup>a, b</sup>, Wenbin Chen <sup>a</sup>, Xinglei Feng <sup>a</sup>, Dong Wang <sup>a</sup>, Chunyan Song <sup>a, b</sup>, Zhongwei Wang <sup>a, c, d</sup>

<sup>a</sup> Chengdu Institute of Geology and Mineral Resources, Chengdu 610081, China

<sup>b</sup> Key Laboratory for Sedimentary Basin and Oil and Gas Resources, Ministry of Land Resources, Chengdu 610081, China

<sup>c</sup> Chinese Academy of Geological Sciences, Beijing 100037, China

<sup>d</sup> China University of Geosciences, Beijing 100083, China

## ARTICLE INFO

### Article history:

Received 14 November 2014

Received in revised form

29 January 2015

Accepted 16 February 2015

Available online 24 February 2015

### Keywords:

Marine oil shale

Redox conditions

Primary productivity

Organic matter accumulation

Qiangtang basin

## ABSTRACT

The organic-rich Changliang Mountain oil shale, located in the North Qiangtang depression, northern Tibet, is considered to be excellent mineral resource in China. The Changliang Mountain oil shale reported here was deposited in a tidal flat-lagoon environment and is characterized by black thin-layered oil shales intercalated with dark-gray marls. Here, we present geochemical data from the Changliang Mountain oil shale profile, in order to investigate the mechanism of organic matter (OM) accumulation and to establish the formation model for the marine oil shale deposition. Total organic carbon (TOC) values range from 2.96 to 23.47% in the oil shale samples, while the marl samples contains low TOC contents, ranging from 0.06 to 0.21%. In the organic-rich oil shale sediments, many redox indicators, including Mo/Al ratios, V/Cr ratios, Th/U ratios, Ni/Co ratios, and the relationship of Mo to TOC suggest a deposition under dysoxic to anoxic environments. Subsequently, the bottom water evolved into an oxic water body when the organic-poor marls were deposited. However, the negative and/or weak relationship between TOC and productivity indices P/Ti and Ba/Al indicates that OM accumulation was not controlled mainly by primary productivity, but dysoxic/anoxic bottom water environment. A stratified water column may be initiated by the supply of fresh water from the continent nearby, combining with warm and humid climate, which is beneficial to the reproduction of marine organisms. The death and bury of these organisms could lead to the formation of dysoxic/anoxic bottom waters and enhance the preservation of OM. In this study, a preservation model of the Changliang Mountain oil shale was established. The model implies that excellent preservation is the major controlling factor for OM enrichment in the oil shale layer. In addition, factors such as mixed deposition with clay minerals, and detrital matter input cannot be ignored for their influence on OM enrichment.

© 2015 Elsevier Ltd. All rights reserved.

## 1. Introduction

Oil shale, as an alternative resource, has received much attention for many years (Dyeni, 2006; Kök, 2006; Liu et al., 2009a). In China, oil shale was formed mainly in lacustrine environments, such as the Tertiary oil shale in Maoming, Huadian and Fushun areas (Liu et al., 2009b), and the Cretaceous oil shale in Songliao

(Wang et al., 1996) and Minhe basins (Liu et al., 2009b). Marine oil shale was mainly found in the Qiangtang basin, northern Tibet, China (Wang and Zhang, 1987; Fu et al., 2008, 2009a, 2009b), including the Bilong Co oil shale and the Shengli River-Changshe Mountain oil shale, representing another large mineral resource in China (Wang et al., 2009a).

The abundance of organic carbon preserved in modern and ancient sedimentary deposits reflects the interplay of various oceanographic and sedimentological conditions, including primary productivity, bottom-water oxygen supply, nutrient availability, the flux of clastic sediment, and the activity of such degradation processes as bacterial sulfate reduction (e.g. Demaison and Moore,

\* Corresponding author. Chengdu Institute of Geology and Mineral Resources, Chengdu 610081, Sichuan, China. Tel.: +86 28 83220166; fax: +86 28 83222657.

E-mail addresses: [zengsq@126.com](mailto:zengsq@126.com) (S. Zeng), [jianwang@mail.sc.cninfo.net](mailto:jianwang@mail.sc.cninfo.net) (J. Wang).

1980; Calvert, 1987; Pedersen and Calvert, 1990; Arthur and Sageman, 1994; Wignall, 1994; Murphy et al., 2000; Wei et al., 2012; Fu et al., 2014; Lash and Blood, 2014; Yan et al., 2015), but by far the main control factor is still controversial. The controversies focus on whether the enrichment of OM is mainly controlled by water column condition (i.e. dysoxia/anoxia condition in the water column and the sedimentation rate) (Canfield, 1989; Ingall et al., 1993; Arthur and Sageman, 1994; Arthur et al., 1998; Mort et al., 2007; Huang et al., 2013), or by primary productivity (Pedersen and Calvert, 1990; Caplan and Bustin, 1998; Sageman et al., 2003; Gallego-Torres et al., 2007; Fu et al., 2014). The preservation model emphasises the importance of dysoxia/anoxia in the water column as the cause of enhanced organic accumulation (Demaison and Moore, 1980). However, the productivity model favors a higher settling flux of organic carbon as the main control on organic accumulation (Wignall and Newton, 2001). Variations in the amount of fine-grained clastic sediment delivered to the basin was shown to influence the concentration of organic matter either by accelerating the rate of passage of organic matter through geochemical zones of intense organic degradation or by diluting the organic matter flux (Ibach, 1982; Sageman et al., 2003; Lash and Blood, 2014). However, it seems that no single control can explain organic accumulation in all sediments, and that each sedimentary setting may have specific factors that contribute to the accumulation of organic-rich sediments (Arthur and Sageman, 1994; Canfield, 1994; Rimmer, 2004; Lash and Blood, 2014; Yan et al., 2015).

The Cretaceous oil shales take place in many areas of the Qiangtang Basin, were generally deposited in a tidal flat-lagoon environment (Fu et al., 2009b; Wang et al., 2010a) and characterized by black thin-layered oil shales intercalated with dark-gray marls (or limestones) (Wang et al., 2009, 2010a; Zeng et al., 2014). Stratigraphy, paleontology, paleoenvironment, paleoclimate and source region of these organic rich oil shales have been well documented (Fu et al., 2009a, 2010a, 2011; Zeng et al., 2012; Wang et al., 2010a). Fu et al. (2007) proposed that the deposition of oil shale was not only associated with sea-level fluctuation but also influenced by paleoclimate, which was the essential reason for formation and disappearance of the oil shale. Wang et al. (2010a) considered the injection recharge of plentiful fresh water and high productivity as the controlling factors for the formation of the oil shales. Although there are some publications about the Early Cretaceous marine oil shales, the factors controlling the enrichment of organic matter have not been well understood.

Trace elements Mo, U, V, Cr, Ni, and Co are enriched in reducing sediments and are highly sensitive to redox changes, making them and their ratios as important proxies for paleoredox reconstruction (Holland, 1978; Piper, 1994; Algeo and Maynard, 2004; Rimmer, 2004; Tribouillard et al., 2006). The oceanic redox changes play an important role in organic matter accumulation (Yan et al., 2015). Under oxic conditions, adsorption to insoluble oxyhydroxides is important, and some dissolved trace elements can become enriched along redox gradients from the oxic water column across the sedimentwater interface to sediments. Such processes are particularly efficient under euxinic condition, where trace element may be precipitated as sulfides or become adsorbed onto OM and insoluble oxyhydroxides (Tribouillard et al., 2006). On the other hand, the contents of barium (Ba), phosphorus (P), and the Ba/Al and P/Ti ratios are used as proxies for paleoproductivity (Dymond et al., 1992, 1996; Ingall et al., 1993; Filippelli and Delaney, 1994; Murray et al., 1993, 1996; Paytan et al., 2007; Algeo et al., 2011; Luo et al., 2012). Dean et al. (1997) proposed Ba/Al to evaluate the paleoproductivity of the laminated sediments in the continental margins of Central California (CCAL) during the last interstadial and Algeo et al. (2011) used excess Ba and P/Ti as paleoproductivity proxies in two Permian/Triassic boundary sections in central Japan.

Large-scale regressions took place in the Qiangtang basin during the Cretaceous time. As a result, a barrier-lagoon system was formed in the Changliang Mountain area when the relative sea level was low. So, the Changliang Mountain area was isolated from the sea by a palaeotopographic high (Marguo Chaka uplift) and then a wide lagoonal area developed behind the protecting barriers (Fu et al., 2009b), where environmental changes were more frequent than normal marine systems and organic-rich oil shales may show strong vertical and horizontal variations in hydrocarbon potentials and geochemical characteristics. The organic-rich oil shale of the Changliang Mountain in the North Qiangtang depression provides a useful example for understanding the redox conditions, paleoproductivity, and the mechanisms of organic matter accumulation. The aim of this paper is to discuss the geochemical characteristics of the oil shale from the Changliang Mountain in the North Qiangtang depression and their implications to organic matter accumulation, and to differentiate the two potential driving mechanisms (i) preservation conditions, (ii) primary productivity for different stata (oil shales or marls) and discuss the formation model of the Cretaceous marine oil shale in the North Qiangtang depression.

## 2. Geological settings

On a large scale, the Tibetan Plateau constitutes a tectonic collage of continental blocks. From north to south, Tibet is comprised of the Kunlun-Qaidam, Songpan-Ganzi flysch complex, Qiangtang, and Lhasa terranes, which are separated by the east striking Anyimaqen-Kunlun-Muztagh, Hoh Xil-Jinsha River and Bangong Lake-Nujiang River suture zones, respectively (Fu et al., 2014) (Fig. 1A). It is generally accepted that the paleo-Tethys represented by the present Jinsha River suture opened possibly in Early Carboniferous time (Yin and Harrison, 2000) and closed by Permian to latest Triassic time (Kapp et al., 2003). The mid-Tethys branch between the Lhasa and Qiangtang terranes was open by Early Jurassic time (Kapp et al., 2003) and closed along the Bangong Lake-Nujiang River suture during the Late Jurassic time (Yin and Harrison, 2000).

The Qiangtang Basin, bounded by Hoh Xil-Jinsha River suture zone to the north and Bangong Lake-Nujiang River suture zone to the south, respectively, consists of the South Qiangtang depression, the central uplift and the North Qiangtang depression (Fig. 1B), which is a Mesozoic marine sedimentary basin overlying folded Paleozoic basement rocks (Wang et al., 2010b) (Fig. 1B). The basin initiated as a foreland basin in the Early Triassic and evolved into a rift basin in the Late Triassic (Fu et al., 2010b; Wang et al., 2010b). At the beginning of the Cretaceous period, the Banggong ocean was closed by the northward subduction beneath the Qiangtang terrane (Kapp et al., 2003), resulting in a large-scale regression in the Qiangtang Basin (Wang et al., 2009b). During this interval, the South Qiangtang depression was uplifted entirely, while the North Qiangtang depression was still a depositional region (Fu et al., 2009b).

The Changliang Mountain oil shale is located in the southern part of the North Qiangtang depression (Fig. 1C), where Lower Cretaceous marine deposits are widespread (Fu et al., 2008), including the upper part of the Suowa Formation, the Xueshan Formation and the Bailong Binghe Formation. On the basis of sedimentary structures, lithology and fossils, three facies associations were recognized: fluvial-delta, tidal flat-lagoon and shallow marine. The Changliang Mountain oil shale was deposited in the tidal flat-lagoon environment.

## 3. Samples and analytical methods

### 3.1. Samples

The studied profile is located in the Changliang Mountain area, the western part of the Shengli River-Changshe Mountain oil shale

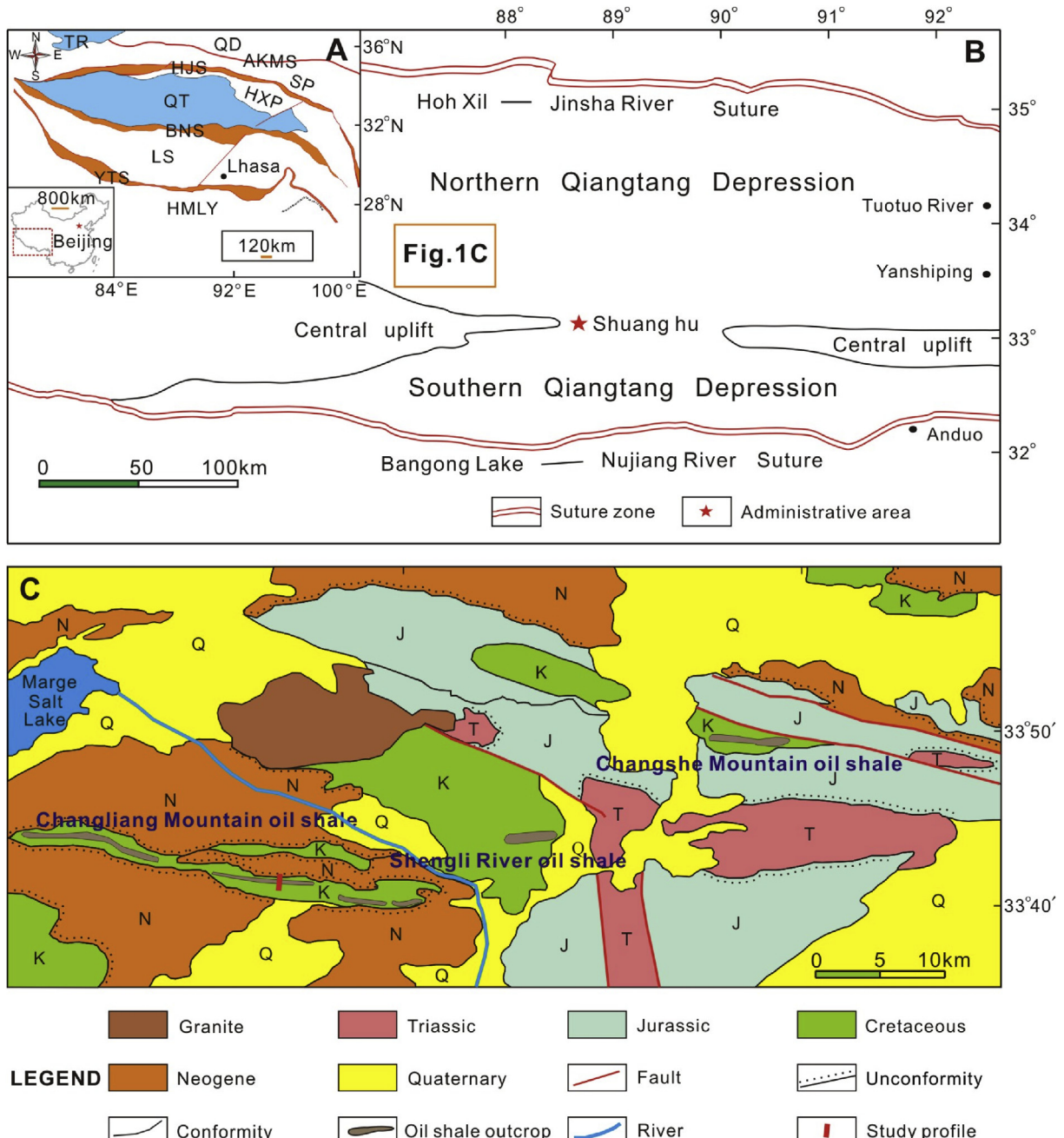


**Figure 1.** (A) Map of the Tibetan Plateau showing major terranes (Modified from Fu et al., 2014). (B) Generalized map, showing the tectonic units of the Qiangtang Basin and the location of study area. (C) Simplified geological map of the Changliang Mountain area, showing location of oil shale section and Mesozoic strata. TR. Tarim basin; QD. Qaidam; AKMS. Anyimaqen-Kunlun-Muztagh suture; HJS. Hoh-Jinsha River suture; SP. Songpan-Ganzi flysch complex; HXP. Hol Xili piedmont zone; QT. Qiangtang basin; BNS. Bangong Lake-Nujiang River suture; LS. Lhasa terrane; YTS. Yarlung Tsangpo suture; HMLY. Himalayas.

zone (Fig. 1C). A total of 21 samples were collected from this section, including 15 oil shale samples and 6 marl samples. These samples were collected from the oil shale seam with a vertical sampling interval of ~1 m on average. All samples were collected and stored in plastic bags to ensure as little contamination and oxidation as possible.

### 3.2. Analytical methods

Total organic carbon (TOC) and organic sulfur ( $S_{o,d}$ ) values were determined at the Geological Laboratory of Exploration and Development Research Institute of PetroChina Southwest Oil and

Gas Field Company, using a LECO analyzer on acidified samples, using a chemical method according to Chinese standards GB/T215-2003 (2003) and GB/T19145-2003(2003), respectively. Pulverized whole-rock samples (2 g) were digested with warm 15%  $HClO_4$ , and  $CO_2$  was released in the process; this digestion was followed by analyses of TOC and  $S_{o,d}$ .

Samples for geochemical analysis were crushed and ground to less than 200 mesh (DZG 20.10-1990 1990; DZ/T 0223-2001 2001). X-ray fluorescence spectrometry (XRF) was used to determine the oxides of major elements, including  $SiO_2$ ,  $Al_2O_3$ ,  $CaO$ ,  $K_2O$ ,  $Na_2O$ ,  $Fe_2O_3$ ,  $MnO$ ,  $MgO$ ,  $TiO_2$ , and  $P_2O_5$ . The analytical procedures are similar to those described by Kimura (1998). The analytical

uncertainty is usually <5%. An inductively coupled plasma mass spectrometer (ICP-MS) was used to determine trace element contents, following Chinese National Standard DZ/T 0223-2001 (2001). For ICP-MS analysis, 25 mg samples are digested with 1-ml HF and 0.5-ml HNO<sub>3</sub> in screw top PTFE-lined stainless steel bombs at 190 °C for 48 h. Insoluble residues are dissolved at 130 °C using 5-ml 30% (v/v) HNO<sub>3</sub> for 3 h, and diluted to 25 ml. The detection limit for elements is 0. n–n × 10<sup>-12</sup> (n = 1–9) (Liu et al., 1996). Selenium and As were determined by atomic fluorescence spectrometry, using the chemical method described in Chinese standard DZG 20.10-1990 (1990).

## 4. Results

### 4.1. Oil shale characteristics

The analytical results of TOC and S<sub>o,d</sub> are listed in Table 1. Based on the lithological data, the Changliang Mountain oil shale succession can be subdivided into four lithostratigraphic units, named A, B, C and D, respectively (Fig. 2).

In Unit A, the TOC contents are very low, with a same content of 0.06% in two marl samples. In Unit B, we observe a major enrichment in organic matter (average 6.37%), varying from 2.96 to 12.21%, with a maximum content of 12.21% in sample CL-3 (Fig. 2). Then, from sample CL-14 to CL-17, the TOC contents drop sharply to a minimum of 0.08%, with an average of 0.12% in Unit C. The bottom of Unit D shows a sharp enrichment in organic carbon up to 13.65% (sample CL-18), and then a gradual increase to maximum of around 23% (sample CL-19 and CL-21) (Fig. 2). The Changliang Mountain oil shales are enriched with organic carbon relative to average shale (AS) (Wedepohl, 1971, 1991), with enrichment factor (EF) of 144 (Fig. 3).

The S<sub>o,d</sub> contents in the oil shale and marl samples from Changliang Mountain area vary between 0.76–1.39% and 0.01–0.37%, respectively (Fig. 2; Table 1). The average S<sub>o,d</sub> contents of the four units is 0.02%, 0.34%, 0.02% and 0.73%, respectively.

### 4.2. Major element geochemistry

Results of major element analysis of samples are listed in Table 1. Marine shales can be regarded as an admixture of three end-

member oxides: SiO<sub>2</sub> (detrital quartz and/or biogenic silica), Al<sub>2</sub>O<sub>3</sub> (clay fraction) and CaO (carbonate content) (Ross and Bustin, 2009). The ternary plot of these major elements indicates that the majority of oil shales examined are variably enriched with CaO (ranging from 24.43 to 49.93%) relative to SiO<sub>2</sub> and Al<sub>2</sub>O<sub>3</sub> (Fig. 4), which is necessarily associated with reduced TOC contents (a good correlation between TOC and CaO,  $r^2 = 0.79$ , Table 2).

Table 1 shows that the most abundant elements are Si, Al, Fe, and Ca. High Ca content may correspond to abundant fossil remains in the oil shale samples. The elements Si, Al, Ti, and K are mainly associated with quartz and clay minerals. Fe<sub>2</sub>O<sub>3</sub> contents range from 1.51 to 5.12% in the oil shale samples. Usually, high Fe<sub>2</sub>O<sub>3</sub> contents are related to abundant Fe-sulfides including siderite, hematite, and pyrite. Like Ti, P, and Mn, K and Na contents are also lower than 1.0% (Table 1). Compared to the oil shale samples, major elements in the marl samples exhibit higher CaO (46.64–52.92%), and lower MgO (0.67–1.02%) contents. The high contents of CaO in the samples are probably related to calcite, abundant bivalve, or gastropod fossil remains, which are generally regarded as the source of Ca.

Sodium concentrations are low in all sediments compared to average shale (AS) (Fig. 3). For AS, the Na content reflects plagioclase which dominate over K-feldspars (Wedepohl, 1971; Ross and Bustin, 2009), indicating the Changliang Mountain oil shale and marl samples contain relatively little plagioclase. Titanium, a diagenetically stable constituent of marine sediment, has an enrichment factor less than 1.0. The good relationship between TiO<sub>2</sub> and Al<sub>2</sub>O<sub>3</sub> ( $r^2 = 0.90$ ; Fig. 5; Table 2) suggests either the occurrence of Ti within clay lattices or that the detrital material came from a constant source (and limited effect of winnowing processes) (Ross and Bustin, 2009).

The chemical index of alteration (CIA) was applied to the paleoclimate reconstruction of sediments (Fedo et al., 1997; Yong and Nesbitt, 1999; Feng et al., 2004; Yan et al., 2010; Sun et al., 2012). The CIA is expressed as: CIA = molar [(Al<sub>2</sub>O<sub>3</sub>)/(Al<sub>2</sub>O<sub>3</sub> + CaO\* + Na<sub>2</sub>O + K<sub>2</sub>O)] × 100, Where CaO\* represents the CaO in silicate minerals only (Nesbitt and Yong, 1982, 1989). In this paper, the CaO was initially corrected for phosphate using available P<sub>2</sub>O<sub>5</sub> data (CaO\* = mole CaO – mole P<sub>2</sub>O<sub>5</sub> × 10/3). If the remaining number of moles is less than that of Na<sub>2</sub>O, the CaO value was adopted as the CaO\*. Otherwise, the CaO\* was assumed to be

**Table 1**

Contents of major-element oxides and the chemical index of alteration (CIA) of the samples in the Changliang Mountain section (in %).

Sample	Lithology	TOC	S <sub>o,d</sub>	SiO <sub>2</sub>	Al <sub>2</sub> O <sub>3</sub>	Fe <sub>2</sub> O <sub>3</sub>	CaO	MgO	K <sub>2</sub> O	Na <sub>2</sub> O	TiO <sub>2</sub>	P <sub>2</sub> O <sub>5</sub>	MnO	CIA
CL-1	Marl	0.06	0.01	8.08	2.08	0.95	48.04	1.02	0.43	0.13	0.12	0.03	0.06	—
CL-2	Marl	0.06	0.02	10.12	2.41	1.07	46.64	0.78	0.52	0.14	0.14	0.05	0.06	—
CL -3	Oil shale	12.21	0.43	13.19	3.08	2.86	33.13	4.29	0.68	0.20	0.18	0.90	0.04	74
CL -4	Oil shale	6.39	0.23	9.19	2.16	3.98	35.58	6.50	0.41	0.25	0.12	0.62	0.06	70
CL -5	Oil shale	4.58	0.28	4.59	1.18	3.43	37.44	8.34	0.24	0.12	0.06	0.52	0.04	71
CL -6	Oil shale	4.06	0.25	4.64	1.23	3.09	38.01	8.34	0.26	0.14	0.06	0.42	0.04	69
CL -7	Oil shale	6.39	0.31	6.30	1.65	2.69	40.13	4.36	0.35	0.18	0.09	0.66	0.03	70
CL -8	Oil shale	5.38	0.29	4.23	1.04	2.04	41.94	5.84	0.24	0.16	0.06	0.49	0.03	65
CL -9	Oil shale	2.96	0.22	2.25	0.70	1.51	49.93	1.47	0.15	0.15	0.03	0.33	0.02	61
CL -10	Oil shale	5.01	0.27	4.20	1.12	2.13	44.56	2.92	0.22	0.14	0.06	0.63	0.02	69
CL -11	Oil shale	11.97	0.73	14.01	3.74	5.12	26.30	6.62	0.84	0.17	0.20	1.18	0.06	76
CL -12	Oil shale	6.03	0.27	5.43	1.34	2.25	39.70	6.64	0.29	0.17	0.07	0.55	0.05	68
CL -13	Oil shale	5.12	0.41	2.64	0.71	2.17	41.67	8.17	0.14	0.11	0.03	0.37	0.04	66
CL -14	Marl	0.10	0.03	2.71	0.61	0.27	52.92	0.67	0.14	0.13	0.03	0.04	0.04	—
CL -15	Marl	0.21	0.02	8.58	2.33	0.85	47.18	0.68	0.46	0.14	0.11	0.02	0.03	—
CL -16	Marl	0.08	0.02	8.00	2.37	0.90	48.14	0.70	0.49	0.14	0.12	0.03	0.04	—
CL -17	Marl	0.09	0.01	8.15	2.30	0.83	48.06	0.69	0.45	0.13	0.12	0.03	0.04	—
CL -18	Oil shale	13.65	0.50	13.05	3.96	3.67	33.14	0.56	0.95	0.19	0.16	0.63	0.03	75
CL -19	Oil shale	23.47	1.11	14.06	4.10	4.70	25.96	0.63	0.93	0.24	0.16	0.72	0.03	74
CL -20	Oil shale	13.42	0.43	7.91	2.34	1.98	39.47	0.35	0.50	0.16	0.09	0.46	0.02	74
CL -21	Oil shale	22.79	0.86	16.45	4.76	4.42	24.46	0.68	1.08	0.22	0.20	0.90	0.03	76

TOC, total organic carbon; S<sub>o,d</sub>, organic sulfur.

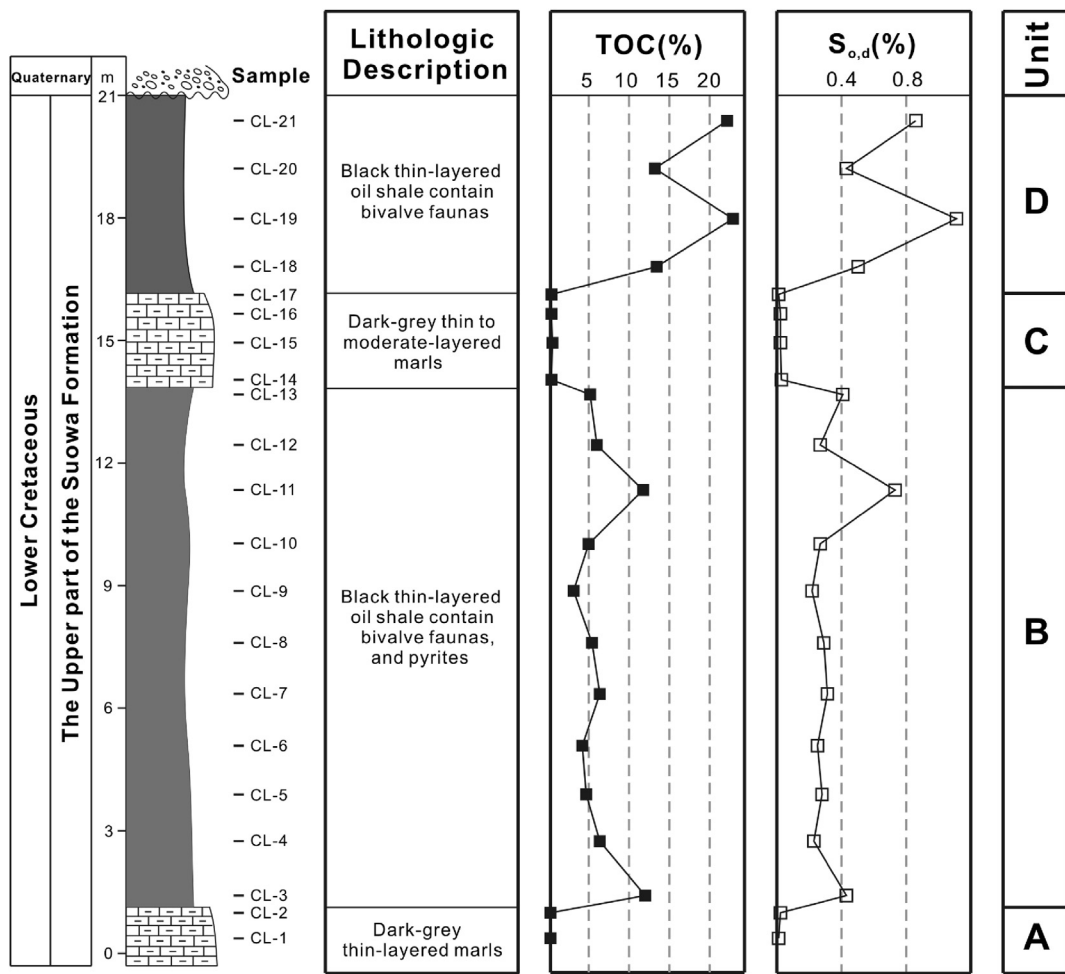


**Figure 2.** Lithostratigraphy (including lithostratigraphic units A to D) and vertical distribution of TOC and organic sulfur ( $S_{o,d}$ ) contents in the Changliang Mountain oil shale profile. Samples are numbered according to depth in the profile.

equivalent to Na<sub>2</sub>O (McLennan, 1993; Yan et al., 2010). The CIA values of the oil shale and marl samples are listed in Table 1. During the oil shale deposition (Units B and D), CIA values vary from 61 to 76 (average 70.6), which are almost lower than those of average

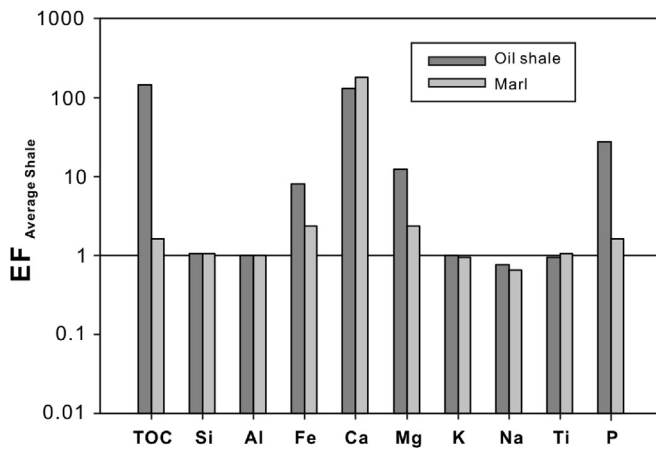


**Figure 3.** Enrichment factors (EFs) of major elements, relative to average shale (Wedepohl, 1971) of TOC and major elements of the oil shales and marls in the Changliang Mountain area. Horizontal line drawn at EF<sub>average shale</sub> = 1 to highlight enrichment or depletion of elements.

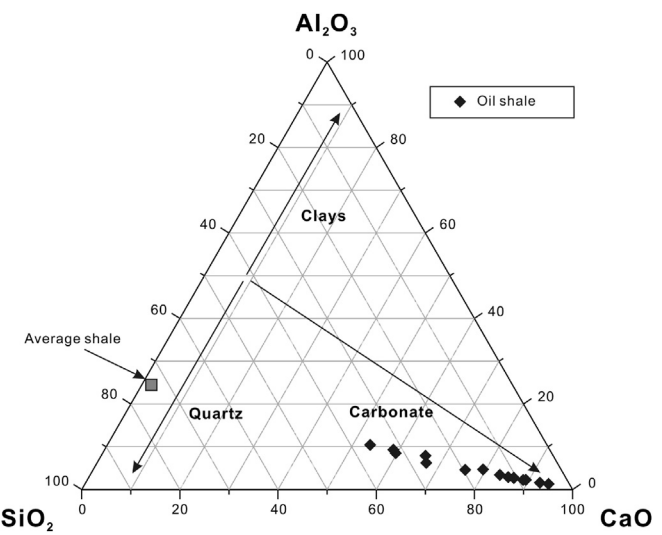


**Figure 4.** Ternary diagram showing relative proportions of major oil shale elements SiO<sub>2</sub> (quartz), Al<sub>2</sub>O<sub>3</sub> (clays) and CaO (carbonates). Average shale also shown as checked box (after Wedepohl, 1971).

**Table 2**

The correlation coefficients of total organic carbon (TOC), organic sulfur and major element content of oil shale and marl from the Changliang Mountain area.

	TOC	S <sub>o,d</sub>	SiO <sub>2</sub>	Al <sub>2</sub> O <sub>3</sub>	Fe <sub>2</sub> O <sub>3</sub>	CaO	MgO	K <sub>2</sub> O	Na <sub>2</sub> O	TiO <sub>2</sub>	P <sub>2</sub> O <sub>5</sub>	MnO
TOC	1.00											
S <sub>o,d</sub>	0.95	1.00										
SiO <sub>2</sub>	0.69	0.60	1.00									
Al <sub>2</sub> O <sub>3</sub>	0.73	0.64	0.98	1.00								
Fe <sub>2</sub> O <sub>3</sub>	0.80	0.85	0.58	0.58	1.00							
CaO	-0.89	-0.89	-0.72	-0.72	-0.95	1.00						
MgO	-0.08	-0.08	-0.33	-0.39	0.39	-0.26	1.00					
K <sub>2</sub> O	0.76	0.67	0.97	0.99	0.60	-0.74	-0.38	1.00				
Na <sub>2</sub> O	0.74	0.64	0.66	0.64	0.69	-0.71	-0.08	0.64	1.00			
TiO <sub>2</sub>	0.58	0.49	0.98	0.95	0.52	-0.66	-0.30	0.93	0.59	1.00		
P <sub>2</sub> O <sub>5</sub>	0.77	0.80	0.49	0.47	0.89	-0.87	0.39	0.50	0.62	0.46	1.00	
MnO	-0.31	-0.26	0.18	0.07	0.01	-0.02	0.33	0.03	-0.03	0.28	-0.09	1.00

shale (70–75) (Nesbitt and Young, 1989, 1996), indicating a low degree of chemical weathering. When plotted in the A–CN–K ( $\text{Al}_2\text{O}_3$ –CaO + Na<sub>2</sub>O–K<sub>2</sub>O) ternary diagram (Fig. 6), sediments produced by intense chemical weathering were plotted in positions commensurate with high CIA values (80–100), whereas incipiently weathered sediments were plotted near the feldspar join (CIA of 50–70) (Yan et al., 2010).

#### 4.3. Trace element geochemistry

The abundance of trace elements of 21 samples from the Changliang Mountain oil shale is presented in Table 3. Furthermore, the average content of trace elements in average shale (Wedepohl, 1971, 1991), and EF is also given in Table 4.

On average, the most abundant trace elements in oil shale samples are Mn (271 µg/g), Ba (117 µg/g), Sr (528 µg/g), and Zn (403 µg/g). The other elements occur in amounts lower than 100 µg/g. Compared with the oil shale samples, the marl samples contain relatively low trace element content with exceptions of Mn and Ce.

Enrichment factor (EF) is used to describe the enrichment of an element in oil shale, which is the ratio of the content of an element in oil shale to the average shale (Wedepohl, 1971, 1991). Enrichment factors for selected trace elements are shown in Figure 7 and Table 4. The trace elements Cd (EF = 17.1), Cs (EF = 1.24), Cu (EF = 4.53), Mo (EF = 24.3), Ni (EF = 3.28), Pb (EF = 5.31), Se (EF = 15.4), Sr (EF = 7.05), U (EF = 4.02), Zn (EF = 17.0) are enriched (Fig. 7; Table 4). Generally, the enrichment of Mo, Pb, Se, and U is consistent with abundant OM and associated Fe-sulfides (mainly

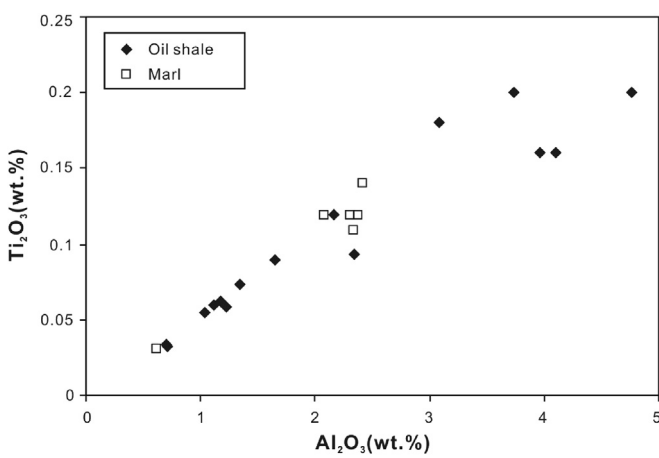


**Figure 5.** Correlation between TiO<sub>2</sub> and Al<sub>2</sub>O<sub>3</sub> suggesting Ti is primarily associated with clay phases.

pyrite) in the oil shale (Fu et al., 2014), and they are hosted mainly in the Fe-sulfides and/or organic matter.

#### 4.3.1. Detrital influx proxies

Titanium, Si, Zr and Th, are considered as indicators of detrital fluxes (Tribouillard et al., 1994; Murphy et al., 2000). Titanium is usually associated with clays and heavy minerals (ilmenite, rutile, etc.), whereas Si is mainly present in both siliciclastic (quartz) and biogenic fractions (Kidder and Erwin, 2001). When normalized to Al, elements such as Si and Ti, which only occur in aluminosilicates, can provide useful information about changes in fluxes derived from detrital non-aluminosilicate sources. The Al-normalized concentrations of Si, Ti, Zr and Th (Fig. 8A) do not show noticeable variation of these elements in Units A, B, and C, excepting the Unit D, which shows slightly lower Si/Al, Ti/Al, and Zr/Al ratios.

It is noteworthy that elements Si, Ti, Zr, and Th concentrations show a similar variation pattern (Fig. 8B). In the lower Unit B, these elements exhibit low concentration (except sample CL-11), and a prominent increase in their concentrations is clearly recorded near the boundary between oil shale (Unit D) and underlying marl layers (Unit C). These data suggest high clastic fluxes derived from detrital aluminosilicate sources during the oil shale deposition, and the detrital fluxes vary through the profile.

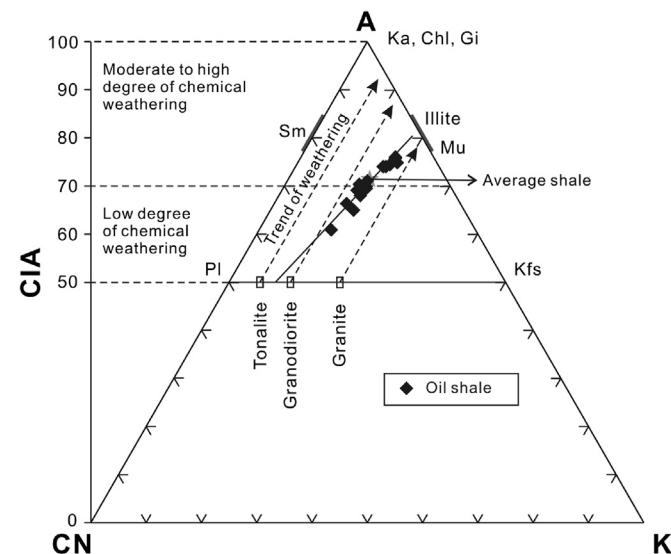


**Figure 6.** Chemical compositional variations in the Changliang Mountain oil shale profile in A–CN–K ( $\text{Al}_2\text{O}_3$ –CaO\* + Na<sub>2</sub>O–K<sub>2</sub>O) ternary diagrams and associated chemical index of alteration (CIA) variations. In triangles, three arrowed solid lines parallel to A–CN sidelines are ideal weathering trends of grandiorite, adamellite and granite. Ka—kaolinite; Chl—chlorite; Gi—Gibbsite; Sm—smectite; Mu—muscovite; Pl—plagioclase; Kfs—K-feldspar.

**Table 3**

Trace element data for organic-rich oil shale and marl samples from the Changliang Mountain section (contents in ppm).

Element	CL-1	CL-2	CL-3	CL-4	CL-5	CL-6	CL-7	CL-8	CL-9	CL-10	
As	3.16	2.68	16.8	26.9	17.2	13.2	10.2	10.1	6.21	6.60	
Ba	53.1	51.3	138	73.2	39.5	42.6	53.6	31.2	25.1	44.0	
Be	0.48	0.46	0.57	0.42	0.29	0.25	0.34	0.26	0.16	0.19	
Cd	0.21	0.11	1.74	1.27	4.85	4.19	1.67	3.86	1.90	0.90	
Ce	14.6	14.4	19.3	12.9	5.75	5.72	7.11	4.96	3.16	4.62	
Co	7.98	7.44	10.3	8.90	7.94	7.75	7.66	8.52	6.73	7.30	
Cr	17.9	17.2	22.7	18.1	15.3	10.0	14.9	9.17	14.5	9.04	
Cs	1.14	1.16	2.17	1.48	0.94	0.96	1.24	0.72	0.47	0.81	
Cu	8.46	8.88	60.8	44.7	34.3	29.4	40.7	31.7	20.1	31.5	
Dy	1.40	1.29	1.37	0.94	0.45	0.44	0.52	0.43	0.25	0.38	
Er	0.74	0.65	0.71	0.59	0.26	0.24	0.28	0.27	0.14	0.22	
Ga	2.90	3.00	4.19	2.91	1.65	1.60	2.06	1.33	0.86	1.44	
Gd	1.50	1.34	1.54	1.10	0.51	0.45	0.60	0.44	0.25	0.40	
Hf	0.69	0.65	1.32	0.77	0.36	0.38	0.52	0.37	0.13	0.42	
La	6.42	6.39	9.26	6.42	2.95	3.00	3.76	2.56	1.66	2.46	
Li	6.37	6.33	11.7	8.21	5.26	5.04	7.13	4.17	2.50	4.47	
Mo	0.31	0.58	16.5	13.3	9.56	7.79	11.9	8.23	8.17	11.3	
Nb	2.51	2.58	3.30	2.39	1.16	1.21	1.69	1.11	0.61	1.09	
Nd	7.02	6.67	8.46	5.47	2.48	2.28	3.08	2.16	1.32	1.91	
Ni	31.5	30.2	58.2	50.3	42.9	40.8	45.4	42.9	41.2	45.0	
P	118	201	3930	270	2270	1834	2882	2139	1441	2751	
Pb	13.3	15.3	19.6	28.7	26.0	33.4	9.24	48.7	19.1	9.04	
Pr	1.66	1.70	2.20	1.45	0.65	0.65	0.81	0.55	0.34	0.53	
Rb	24.7	26.8	35.0	25.6	14.5	14.2	19.9	12.2	7.72	13.0	
Sc	4.27	4.19	4.06	3.39	2.61	2.24	2.79	2.51	1.99	2.40	
Se	0.24	0.21	2.65	2.64	2.92	2.49	3.33	2.41	1.43	1.65	
Sm	1.55	1.50	1.61	1.10	0.48	0.47	0.61	0.42	0.26	0.37	
Sn	0.88	0.89	0.99	0.85	0.73	0.68	0.78	0.67	0.69	0.70	
Sr	280	240	308	280	463	449	630	622	1438	784	
Ta	0.19	0.20	0.26	0.16	0.09	0.09	0.12	0.08	0.05	0.07	
Tb	0.23	0.22	0.24	0.16	0.07	0.07	0.09	0.07	0.05	0.06	
Th	1.85	2.00	2.70	1.90	0.93	1.00	1.26	0.82	0.49	0.77	
U	1.08	1.47	4.22	3.72	2.13	2.12	2.74	3.21	1.89	2.48	
V	26.2	26.7	47.2	41.9	29.5	27.4	32.9	26.5	21.6	29.9	
Y	7.88	7.28	7.90	5.87	2.74	2.60	3.26	2.93	1.64	2.63	
Yb	0.64	0.59	0.63	0.49	0.24	0.22	0.27	0.21	0.13	0.20	
Zn	33.7	23.6	197	208	562	398	232	313	191	108	
Zr	28.6	26.9	56.8	36.8	17.7	15.8	24.1	16.1	6.89	19.3	
U/Al	0.98	1.15	2.59	3.25	3.41	3.26	3.14	5.83	5.10	4.18	
Mo/Al	0.03	0.05	1.01	1.16	1.53	1.20	1.36	1.49	2.20	1.91	
V/Al	2.38	2.09	2.89	3.66	4.72	4.21	3.77	4.81	5.83	5.04	
V/Cr	1.46	1.55	2.08	2.31	1.93	2.74	2.21	2.89	1.49	3.31	
Th/U	1.71	1.36	0.64	0.51	0.44	0.47	0.46	0.26	0.26	0.31	
Ni/Co	3.95	4.06	5.65	5.65	5.40	5.26	5.93	5.04	6.12	6.16	
V/(V + Ni)	0.45	0.47	0.45	0.45	0.41	0.40	0.42	0.38	0.34	0.40	
V/Sc	6.14	6.37	11.63	12.36	11.30	12.23	11.79	10.56	10.85	12.46	
P/Ti	0.16	0.24	3.64	3.76	6.10	5.18	5.34	6.48	7.28	7.64	
Ba/Al	48.2	40.2	84.6	64.0	63.2	65.4	61.4	56.7	67.7	74.2	
La <sub>N</sub> /Yb <sub>N</sub>	—	—	1.42	1.27	1.19	1.32	1.35	1.18	1.24	1.19	
Element	CL-11	CL-12	CL-13	CL-14	CL-15	CL-16	CL-17	CL-18	CL-19	CL-20	CL-21
As	35.8	14.9	8.98	0.31	1.63	2.25	1.04	15.0	22.9	6.85	17.5
Ba	97.5	52.0	46.7	28.9	46.0	60.6	68.2	446	271	106	281
Be	0.76	0.33	0.17	0.17	0.48	0.54	0.47	0.74	0.73	0.43	0.81
Cd	6.42	3.59	5.81	0.30	0.58	0.08	0.05	1.66	7.82	3.39	1.97
Ce	18.2	7.21	2.66	4.52	14.5	14.3	13.9	16.4	16.6	11.0	20.5
Co	13.1	9.06	6.84	5.30	8.61	6.70	7.06	10.4	11.9	9.09	11.9
Cr	26.4	11.2	10.4	6.38	21.2	17.2	19.2	28.7	28.9	20.0	33.5
Cs	2.76	1.00	0.50	0.42	1.16	1.24	1.26	3.51	3.28	1.93	3.81
Cu	84.1	36.3	22.9	9.92	8.41	7.75	8.21	74.2	99.5	55.7	100
Dy	1.12	0.53	0.21	0.39	1.43	1.23	1.12	1.33	1.30	0.90	1.60
Er	0.67	0.28	0.13	0.21	0.73	0.68	0.67	0.77	0.75	0.49	0.89
Ga	4.84	1.80	1.01	0.82	2.89	2.82	2.85	5.08	4.90	2.99	5.67
Gd	1.32	0.47	0.22	0.45	1.46	1.43	1.37	1.46	1.38	0.94	1.75
Hf	1.11	0.44	0.19	0.18	0.62	0.56	0.55	0.73	0.71	0.44	0.91
La	9.12	3.83	1.41	2.07	6.47	6.56	6.41	8.48	8.58	5.74	10.9
Li	13.9	5.43	2.62	1.87	6.63	6.16	6.31	13.9	14.6	9.55	17.9
Mo	21.5	10.5	6.64	0.40	0.23	0.28	0.38	23.6	31.1	19.9	33.9
Nb	3.89	1.37	0.69	0.62	2.29	2.29	2.50	3.13	3.25	1.88	3.80
Nd	7.61	3.13	1.21	2.35	6.78	6.56	6.47	6.56	6.89	4.45	8.66
Ni	69.4	45.0	40.0	25.8	30.5	28.7	29.1	76.6	86.6	65.5	86.5
P	5152	2401	1615	162	100	135	144	2751	3144	2008	3930
Pb	61.1	65.8	31.7	9.67	22.8	2.89	3.52	12.8	18.5	5.19	15.7

(continued on next page)

**Table 3** (continued)

Element	CL-11	CL-12	CL-13	CL-14	CL-15	CL-16	CL-17	CL-18	CL-19	CL-20	CL-21
Pr	1.97	0.79	0.29	0.54	1.69	1.65	1.59	1.74	1.81	1.22	2.21
Rb	47.3	16.5	7.90	7.41	27.2	26.0	25.6	53.4	51.8	30.6	61.4
Sc	4.75	2.80	2.12	2.37	4.23	3.70	3.98	5.04	4.93	3.56	5.23
Se	3.45	2.45	1.84	0.69	0.22	0.83	1.17	2.25	2.30	1.70	2.25
Sm	1.54	0.59	0.24	0.46	1.58	1.37	1.27	1.34	1.32	0.96	1.76
Sn	1.11	0.73	0.65	0.65	0.89	0.94	0.90	1.14	1.07	0.93	1.22
Sr	188	495	386	286	241	279	297	517	305	780	277
Ta	0.25	0.11	0.05	0.05	0.18	0.17	0.19	0.23	0.24	0.14	0.27
Tb	0.22	0.08	0.05	0.07	0.22	0.20	0.19	0.22	0.21	0.15	0.26
Th	3.08	1.13	0.43	0.47	2.06	1.75	1.83	2.90	2.79	1.64	3.34
U	8.26	4.58	1.62	1.28	0.82	0.55	1.14	4.17	5.68	3.48	5.74
V	55.2	28.8	20.3	13.1	25.0	28.3	27.3	70.7	94.1	47.1	87.7
Y	7.37	3.21	1.78	2.50	7.68	7.23	6.80	7.89	8.17	5.61	9.99
Yb	0.61	0.26	0.11	0.16	0.59	0.55	0.57	0.66	0.68	0.41	0.77
Zn	875	293	668	14.4	30.6	7.45	12.8	376	905	435	279
Zr	50.6	20.9	11.4	8.25	27.8	23.5	23.8	31.5	30.7	18.8	38.5
U/Al	4.17	6.46	4.31	3.96	0.66	0.44	0.94	1.99	2.62	2.81	2.28
Mo/Al	1.09	1.48	1.77	0.12	0.02	0.02	0.03	1.13	1.43	1.61	1.35
V/Al	2.79	4.06	5.40	4.06	2.03	2.26	2.24	3.37	4.34	3.80	3.48
V/Cr	2.09	2.57	1.95	2.05	1.18	1.65	1.42	2.46	3.26	2.36	2.62
Th/U	0.37	0.25	0.27	0.37	2.51	3.18	1.61	0.70	0.49	0.47	0.58
Ni/Co	5.30	4.97	5.85	4.87	3.54	4.28	4.12	7.37	7.28	7.21	7.27
V/(V + Ni)	0.44	0.39	0.34	0.34	0.45	0.50	0.48	0.48	0.52	0.42	0.50
V/Sc	11.6	10.3	9.58	5.53	5.91	7.65	6.86	14.0	19.1	13.2	16.8
P/Ti	4.29	5.48	8.41	0.87	0.15	0.19	0.20	2.87	3.27	3.60	3.27
Ba/Al	49.2	73.3	124.2	89.5	37.3	48.3	56.0	212	125	85.6	112
La <sub>N</sub> /Yb <sub>N</sub>	1.45	1.43	1.24	—	—	—	—	1.24	1.22	1.36	1.37

**Table 4**

Average concentrations of Al elements and trace metals of Changliang Mountain oil shale section.

Oxide/lement	Average shale <sup>a</sup>		Oil shale (n = 15)			Marl (n = 6)		
	Abundance	-/Al	Abundance	-/Al	EF	Abundance	-/Al	EF
TOC	0.20	0.03	9.56	4.33	144	0.10	0.05	1.65
SiO <sub>2</sub>	58.9	3.53	8.14	3.68	1.04	7.61	3.77	1.07
Al <sub>2</sub> O <sub>3</sub>	16.7	1.00	2.21	1.00	1.00	2.02	1.00	1.00
Fe <sub>2</sub> O <sub>3</sub>	2.80	0.17	3.07	1.39	8.17	0.81	0.40	2.36
CaO	2.20	0.13	36.8	16.6	128	48.5	24.0	185
MgO	2.60	0.16	4.38	1.98	12.4	0.76	0.37	2.34
K <sub>2</sub> O	3.60	0.22	0.49	0.22	1.00	0.42	0.21	0.93
Na <sub>2</sub> O	1.60	0.10	0.17	0.08	0.78	0.14	0.07	0.67
TiO <sub>2</sub>	0.78	0.05	0.11	0.05	0.95	0.11	0.05	1.06
P <sub>2</sub> O <sub>5</sub>	0.16	0.01	0.63	0.28	28.3	0.03	0.02	1.63
Mn	850	96.2	271	122	1.27	345	171	1.77
Ba	580	65.6	116	52.7	0.80	51.35	25.4	0.39
Be	3.00	0.34	0.43	0.19	0.57	0.43	0.21	0.63
Cd	0.80	0.09	3.40	1.54	17.11	0.21	0.11	1.17
Ce	95.0	10.7	10.4	4.71	0.44	12.7	6.29	0.59
Co	19.0	2.15	9.16	4.14	1.93	7.18	3.56	1.65
Cr	90.0	10.2	18.2	8.23	0.81	16.5	8.17	0.80
Cs	5.50	0.62	1.71	0.77	1.24	1.06	0.53	0.85
Cu	45.0	5.10	51.1	23.1	4.53	8.61	4.26	0.84
Ga	19.0	2.10	2.82	1.28	0.61	2.55	1.26	0.60
Hf	2.80	0.32	0.59	0.27	0.83	0.54	0.27	0.84
La	40.0	4.50	5.34	2.42	0.54	5.72	2.83	0.63
Mo	2.60	0.29	15.6	7.06	24.3	0.36	0.18	0.62
Nb	18.0	2.00	2.04	0.92	0.46	2.13	1.06	0.53
Ni	68.0	7.70	55.8	25.2	3.28	29.3	14.5	1.88
Pb	20.0	2.30	27.0	12.2	5.31	11.3	5.57	2.42
Rb	140	15.8	27.4	12.4	0.78	23.0	11.4	0.72
Se	0.60	0.07	2.38	1.08	15.4	0.56	0.28	3.96
Sr	300	33.9	528	239	7.05	271	134	3.95
Ta	2.00	0.23	0.14	0.06	0.28	0.16	0.08	0.35
Th	12.0	1.40	1.68	0.76	0.54	1.66	0.82	0.59
U	3.70	0.42	3.74	1.69	4.02	1.06	0.52	1.25
V	130	14.7	44.1	19.9	1.36	24.4	12.1	0.82
Y	41.0	4.60	4.91	2.22	0.48	6.56	3.25	0.71
Zn	95.0	10.7	403	182	17.0	20.4	10.1	0.94
Zr	160	18.1	26.4	11.9	0.66	23.1	11.5	0.63

Averages are shown normalized to Al.

<sup>a</sup> Average shale composition from Wedepohl (1971, 1991) used to determine enrichment factors (EF).

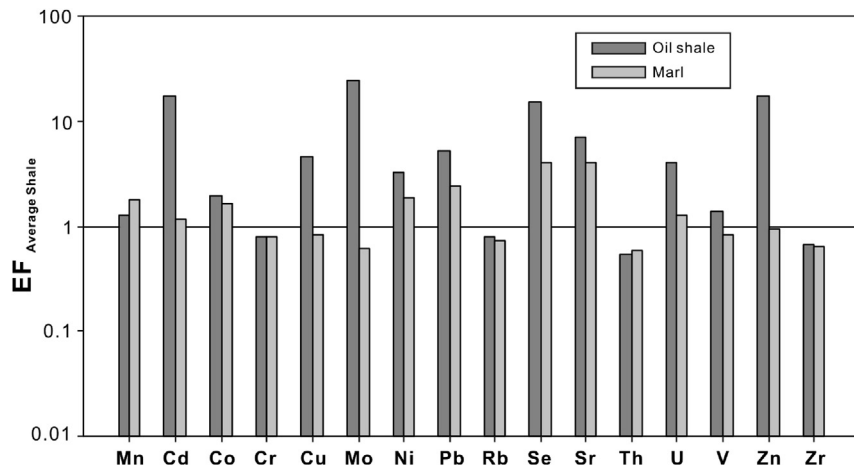


**Figure 7.** Enrichment factors (EF) of trace elements, relative to average shale (Wedeeph, 1971) in the Changliang Mountain area. Horizontal line drawn at  $EF_{\text{average shale}} = 1$  to highlight enrichment or depletion of elements.

#### 4.3.2. Redox sensitive elements

Molybdenum, U and V are considered as redox-sensitive elements (Calvert and Pedersen, 1993; Crusius et al., 1996; Dean et al., 1997; Algeo and Maynard, 2004). A significant feature of the Changliang Mountain oil shale section is the remarkable enrichment in Al-normalized concentrations of these elements in Units B and D (Fig. 9), in comparison with the marl samples in Units A and C. The concentrations of Mo, U, and V display the same trend (Fig. 10). High values of U and V suggest that the sediments were probably O<sub>2</sub>-deficient (Lézin et al., 2013). Similar trends are followed by other paleoenvironment proxies, such as V/Cr, U/Th, Ni/Co, V/(V + Ni) and V/Sc, which were considered as reliable redox indexes (Fig. 9).

In Units A and C, V/Cr is lower than 2, while in Units B and D, it is generally higher than 2 (Fig. 9 and Table 3). The Th/U ratio has been used as a proxy for the redox condition of the depositional environment (Myers and Wignall, 1987; Wignall, 1994). In the Changliang Mountain oil shale section, the Th/U ratios in the oil shale Units B and D range from 0.26 to 0.70, while in the non-oil shale Units A and C, the ratios are generally close to 2, with an except of sample CL-14 (Fig. 9 and Table 3).

#### 4.3.3. Paleoproductivity proxies

Nitrogen and P are the most important nutrient elements for plankton. Plaeoproductivity in marine environments is mainly controlled by the availability of N and P. Phosphorus is regarded as the ultimate limiting factor in marine environments and a major constitute of skeletal material and plays a fundamental role in many metabolic processes (Tyrrell, 1999; Tribouillard et al., 2006), so the content of phosphorus was widely used as an indicator for paleoproductivity. In order to mitigate the dilution effect of OM and authigenic minerals on the absolute content of P in terrigenous detrital matter, P/Ti or P/Al is used to evaluate the plaeoproductivity, because Ti and Al generally originates from terrigenous detrital matter. In the present study, P/Ti ratios are given in Table 3. In the lower subunit A, P/Ti ratios of two samples are 0.16 and 0.24 (Table 3), respectively. In the oil shale Units B and D, P/Ti ratios are generally high, ranging from 3.64 to 8.41 and 2.87 to 3.60 (Table 3), with a mean of 5.78 and 3.25, respectively. These means are higher than those of the cherts (0.34) and the black shales in the Ubara (Algeo et al., 2011), which were thought to be a character of a high paleoproductivity during their deposition. In the non-oil shale Unit C, P/Ti ratios fall between 0.15 and 0.87, with a mean of 0.35, which is similar to that of the cherts (0.34) in the Ubara (Algeo et al., 2011).

The barite accumulation rate shows a positive correlation with primary productivity in the marine sediments (Dymond et al., 1992, 1996; Paytan et al., 1996). Dean et al. (1997) suggested Ba/Ti or Ba/Al ratio can be used to qualitatively assess the paleoproductivity. Titanium or Al is also used as the denominator in order to eliminate the dilution effect of other components. So, both ratios may represent the amount of organisms in the ancient sea. The Ba/Al ratios are list in Table 3. In the oil shale Units B and D, the Ba/Al ratios range from 49.2 to 124 and 85.6 to 212, with a mean of 71.3 and 134, respectively. However, in the non-oil shale Units A and C, the Ba/Al ratios range from 40.2 to 48.2 and 37.3 to 89.5, averaging 44.2 and 57.8, respectively.

## 5. Discussion

### 5.1. Redox conditions

Samples from Changliang Mountain oil shale profile exhibit a wide range of Th/U ratios, ranging from 0.26 to 3.18, which suggests frequent fluctuations in paleoenvironment. Wignall and Twitchett (1996) suggested that anoxic environment yielded Th/U ratios of 0–2 in the shale, and this criteria has been widely accepted in subsequent studies (Wignall and Twitchett, 1996; Kimura and Watanabe, 2001; Yan et al., 2009). All marine oil shale samples from Changliang Mountain profile exhibit low Th/U ratios less than 2, with extreme Th/U ratios as low as 0.26 (Fig. 9), this scenario suggest a more reducing environment at Changliang Mountain section. However, the Th/U ratios of the marl samples yield higher values than the oil shale samples (Fig. 9), suggesting a more oxic bottom waters condition.

In addition, the V systematics (V/Sc, V/Cr, V/(V + Ni)) and Ni/Co ratios are also usually used as proxies for the redox conditions of the depositional environment (Hatch and Leventhal, 1992; Jones and Manning, 1994; Rimmer, 2004; Yan et al., 2009). Although the classification of redox conditions varies in literatures, the basic fact remains that V/Sc, V/Cr, and V/(V + Ni) ratios decrease with increasing oxygenic level in water columns. Vanadium is also a redox-sensitive element that is preferentially concentrated in sediments underlying anoxic or near-anoxic waters. The degree of V enrichment is most efficiently expressed if the V concentration is normalized by Sc abundance, because both V and Sc are insoluble and V varies in proportion to Sc, and environments which characterized by anoxic conditions resulted in significant V enrichment over Sc (Kimura and Watanabe, 2001). Jones and Manning (1994)

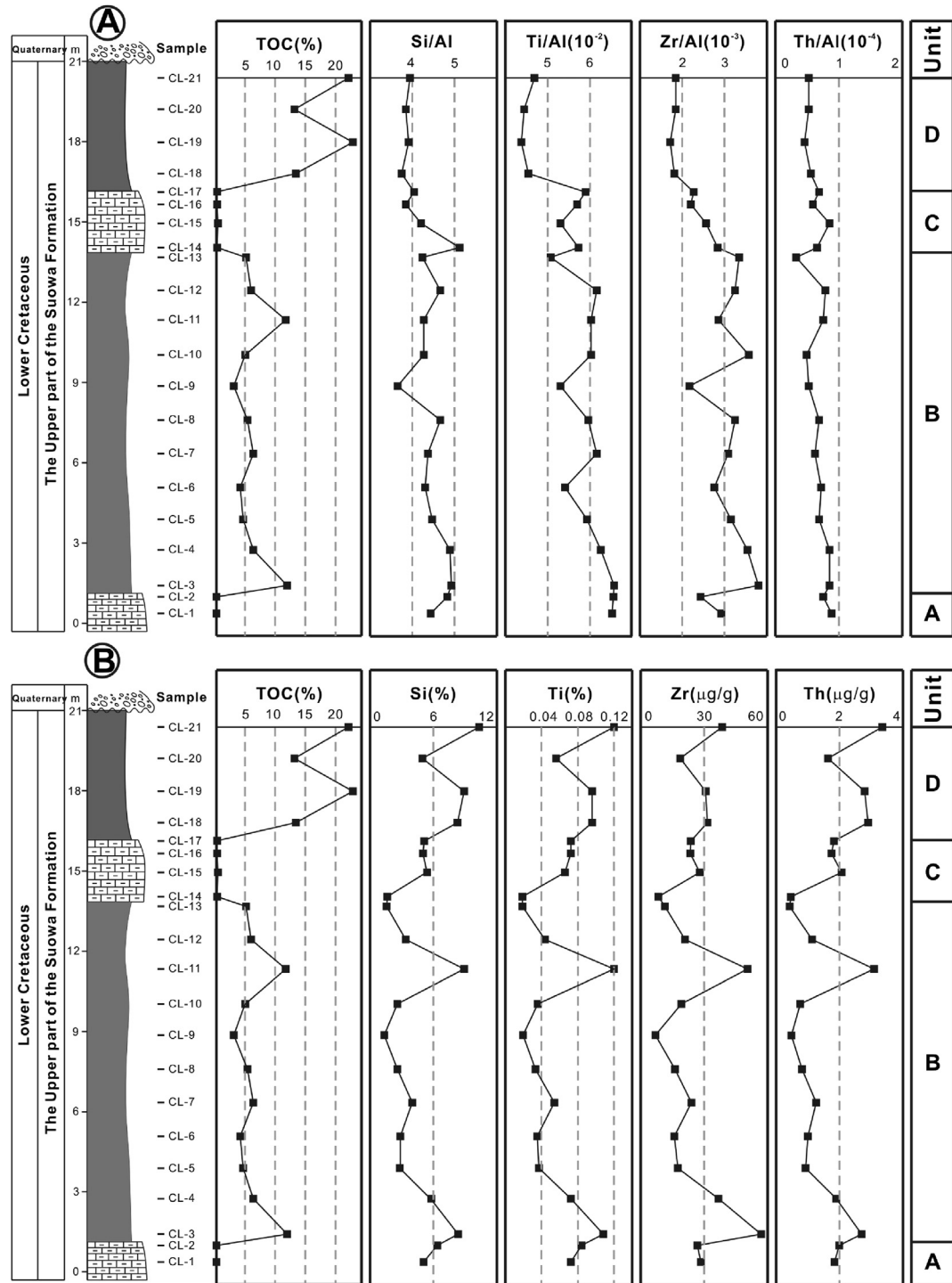


**Figure 8.** Stratigraphic distribution of detrital influx and fresh water influx proxies and TOC contents in the Changliang Mountain oil shale section.

proposed that V/Cr ratios < 2 points to oxic conditions, 2–4.25 to dysoxic conditions, and >4.25 to suboxic to anoxic conditions. In Figure 9, the V/Cr and V/Sc ratios are generally more than 2 and 10 of oil shale Units B and D (Fig. 9), respectively, indicating a dysoxic to anoxic bottom waters environment. However, the V/(V + Ni) ratios show different trends here. V/(V + Ni) predicts oxic condition in oil shale Unit B and dysoxic condition in Unit D (Fig. 11A, and D). These elements are subject to more complex processes controlled by provenance, climate and depositional and diagenetic conditions,

so these redox-sensitive elements should be used with caution when reflecting redox conditions.

In Figure 9, we can see a fairly good agreement from the Th/U and Ni/Co ratios. In Units B and D, the Th/U ratios are generally less than 1.0, indicating anoxic bottom water condition, while the marls in Units A and C are almost more than 1.5, indicating more oxic condition.

Generally, crossplots of trace element ratios (e.g. V/(V + Ni) vs. Th/U, V/Cr vs. Th/U, V/Sc vs. Th/U, V/Sc vs. V/Cr, V/(V + Ni) vs. V/Cr,

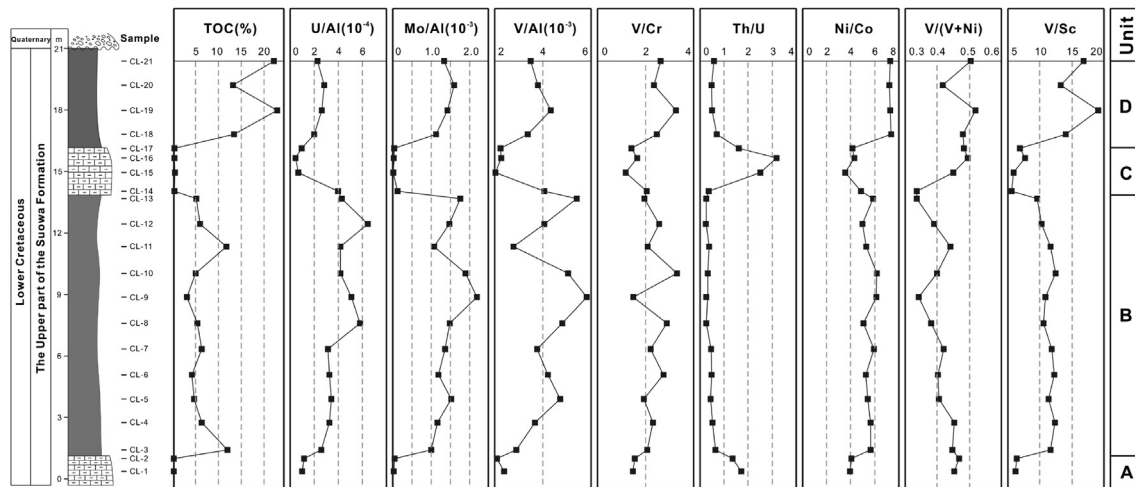


**Figure 9.** Stratigraphic distribution of TOC and Al-normalized trace-element (redox/oxygenation and productivity proxies) contents in the Changliang Mountain oil shale section.

and Ni/Co vs. V/Cr) are used as paleoredox proxies (Fig. 11). The oil shale samples from Units B and D almost fall into the dysoxic to anoxic field, while the marl samples from Units A and C generally fall into the oxic field (Fig. 11).

Molybdenum is a trace element that is very sensitive to redox conditions. Its solubility decreases with increasing reducing conditions (Lézin et al., 2013). The enrichment of Mo is also attributed to adsorption on OM (Algeo and Maynard, 2004; Scott et al., 2008). Mo is only enriched in euxinic environment, so it was regarded as the best diagnosis to distinguish anoxic and euxinic environments (Meyer et al., 2008). In Figure 9, the Mo/Al ratios with depth are in similar trend with TOC, V/Cr, and V/Sc. The Mo contents of the marl samples are very low, in the range of 0.23–0.58 ppm, indicating no enrichment of Mo. However, in the oil shale Units B and D, the Mo contents are higher, ranging from 6.64 to 33.9 ppm, indicative of sediments deposited under anoxic conditions (Crusius et al., 1996; Helz et al., 1996; Dean et al., 1997; Brumsack, 2006; Ross and Bustin, 2009). In oxic seawater, Mo is present as stable  $\text{MoO}_4^{2-}$  (Broecker and Peng, 1982). Below the oxic–anoxic interface, Mo was released to pore water because of

the reductive dissolution of Mn-oxyhydroxide particles (Crusius et al., 1996). Helz et al. (1996) proposed that one  $\text{S}^{2-}$  can replace one  $\text{O}^{2-}$  in  $\text{MoO}_4^{2-}$  in the presence of  $\text{H}_2\text{S}$  to create thiomolybdates ( $\text{MoO}_x\text{S}_{4-x}^{2-}$ ,  $x = 0–3$ ), which makes Mo become a particle-reactive species and then can be enriched in the sediments (Calvert and Pedersen, 1993; Algeo and Maynard, 2004).

A crossplot for Mo, U, and V versus TOC shows a combination of linear correlation and scatter for the Changliang Mountain oil shale samples (Fig. 12). There is a good correlation of TOC to Mo, U, and V content ( $r = 0.98$ , 0.68, and 0.97, respectively), indicating the dysoxic to anoxic bottom water environments played an important role during the organic-rich oil shale deposition.

## 5.2. Biotic productivity

Phosphorus is transferred to the sediment mainly as organically bound P, most of which is subsequently liberated through remineralization of OM, and long-term retention of P in the sediment requires adsorption onto FeOOH phases and subsequent precipitation of authigenic phosphate minerals (Algeo and Ingall, 2007;

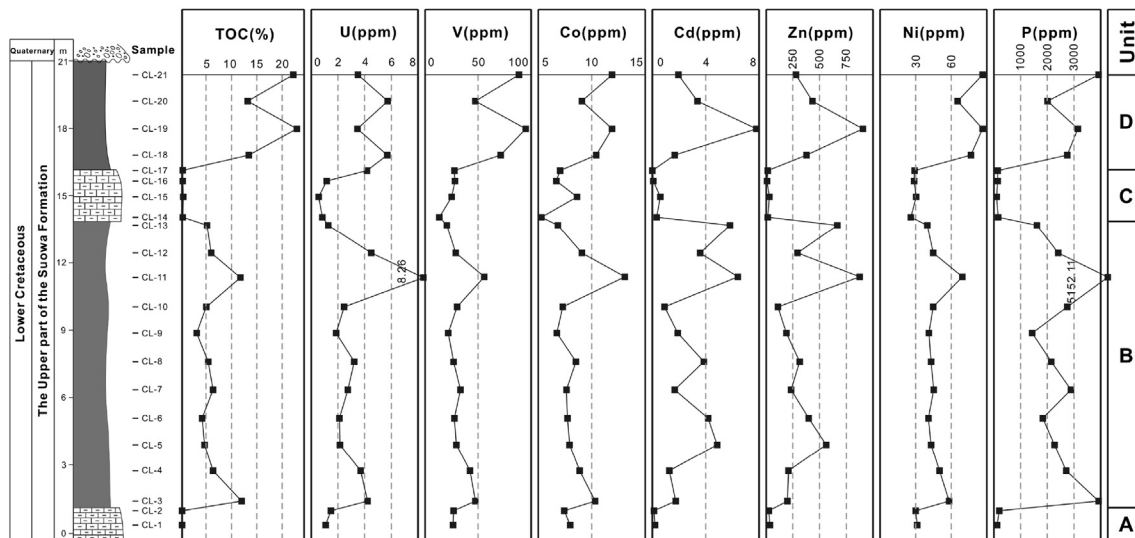


**Figure 10.** Stratigraphic distribution of redox-sensitive element (Co, Cd, P, Ni, Zn, V and U) and TOC contents in the Changliang Mountain oil shale section. Cd, P, Ni and Zn behave as micronutrients (Calvert and Pedersen, 1993; Algeo and Maynard, 2004).

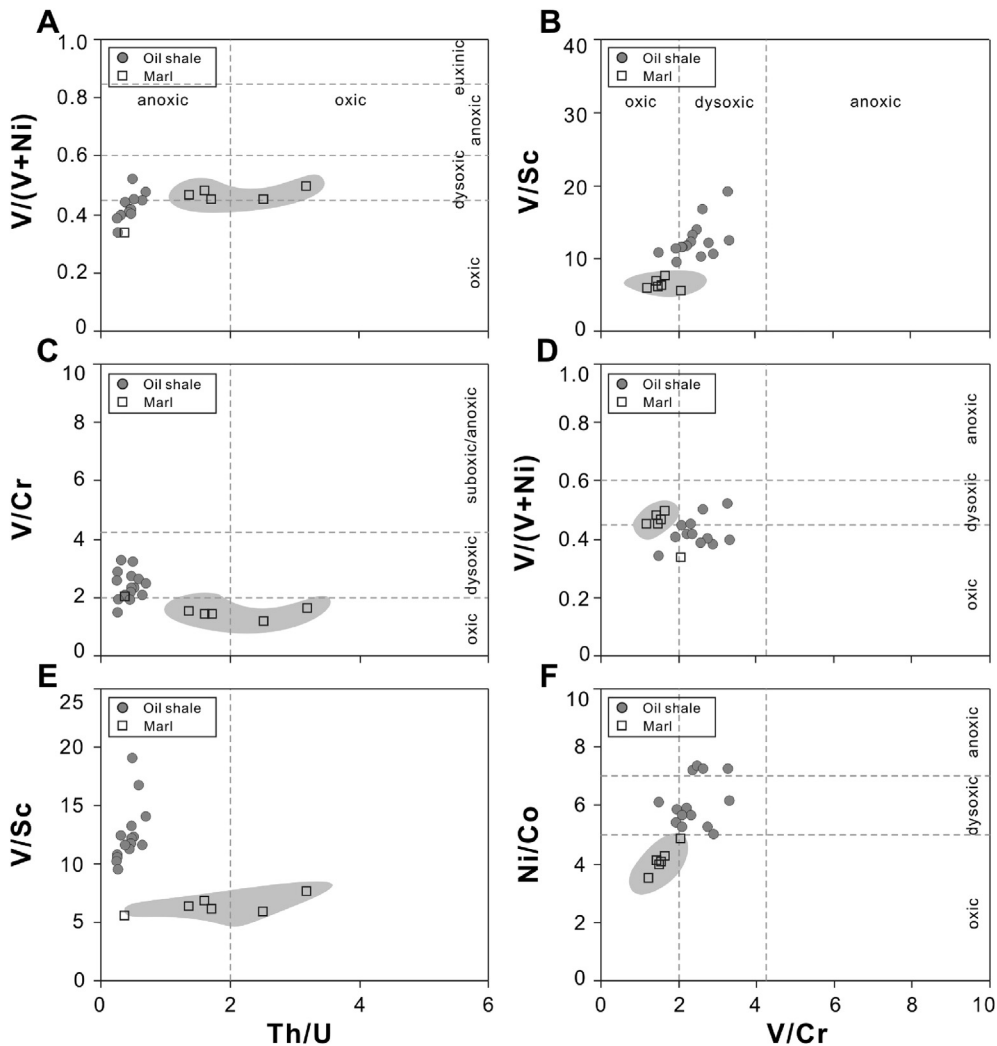


**Figure 11.** Crossplots of trace element ratios used as paleoredox proxies. A:  $V/(V + Ni)$  vs.  $Th/U$ ; B:  $V/Sc$  vs.  $V/Cr$ ; C:  $V/Cr$  vs.  $Th/U$ ; D:  $V/(V + Ni)$  vs.  $V/Cr$ ; E:  $V/Sc$  vs.  $Th/U$ , and F:  $Ni/Co$  vs.  $V/Cr$ . Boundaries of different redox environments from Jones and Manning (1994) for  $Th/U$ ,  $Ni/Co$  and  $V/Cr$ , and Hatch and Leventhal (1992) for  $V/(V + Ni)$ .

(Algeo et al., 2011). P/Ti ratios are used to evaluate the nutrient condition of the ancient sea (Algeo et al., 2011; Luo et al., 2012). In Unit A, P/Ti ratios (average 0.2) (Table 3 and Fig. 13) are close to those for Post Archean Australian Shale (PAAS) (0.13) and average pelagic clay (0.33) and far below those (~2–8) associated with regions of elevated productivity in the modern equatorial Pacific (Murray et al., 1993). The low P/Ti ratios indicate a poor paleoproductivity during the marl deposition. However, in Unit B, the oil shale samples exhibit high P/Ti ratios (average 5.78) (Fig. 13), which are increasing with depth to the peak value 8.43 (sample CL-13) with a few samples (sample CL-11 and CL-12) yielding low values 4.29 and 5.48 (Fig. 13). The high P/Ti ratios were thought to be a character of a high paleoproductivity during their deposition. However, the contents of TOC of the oil shales in section 1 showed the opposite trend with the P/Ti ratios (Fig. 13), which are decreasing with depth to the low value 2.96 (sample CL-9), excepting the sample CL-11 (with a high value 11.97). In section 2, the P/Ti ratios dropped to around 0.20, indicating a low paleoproductivity. Nevertheless, the P/Ti ratios of the oil shale samples in section 3 increase to about 3.0, while the content of TOC are ranging between 13.42 and 23.47%. There is no correlation of TOC and P/Ti ratios ( $r = -0.74$ ) (Fig. 14), showing that the high content of TOC may not mainly be controlled by the primary paleoproductivity, but

may be affected by redox and terrigenous detrital matter influx. The retention of P in the sediment is influenced by two factors: (1) porewater redox condition, and (2) the availability of Fe compounds for absorption of P (Algeo and Ingall, 2007). As mentioned above, the dysoxic to anoxic bottom waters during the Changliang Mountain oil shale deposition probably favored the retention of P liberated from OM, rather than the mineral Fe concentrations.

A second geochemical proxy to qualitatively assess the paleoproductivity is the Ba/Al ratio (Dean et al., 1997). The barite accumulation rate shows a positive correlation with primary productivity in the marine sediments (Dymond et al., 1992, 1996; Paytan et al., 1996, 2007). Within the studied section, the averages of Ba/Al ratios for the Units A and C are lower than the laminated sediments in the continental margins of Central California (CCAL) cores (100–120), which were deposited under a high paleoproductivity (Dean et al., 1997). In Unit B, the Ba/Al ratios increase to around 70 (except sample CL-13, the Ba/Al ratio is 124), indicating a moderate paleoproductivity. The Ba/Al ratios in Unit D are highest of the four units (average is 134), compared to the Ba/Al ratios (around 100–120) of laminated sediments in CCAL cores, which were regarded to be deposited under a high paleoproductivity, the Ba/Al ratios of the oil shale sediments from the Changliang Mountain oil shale are generally higher, while the marl

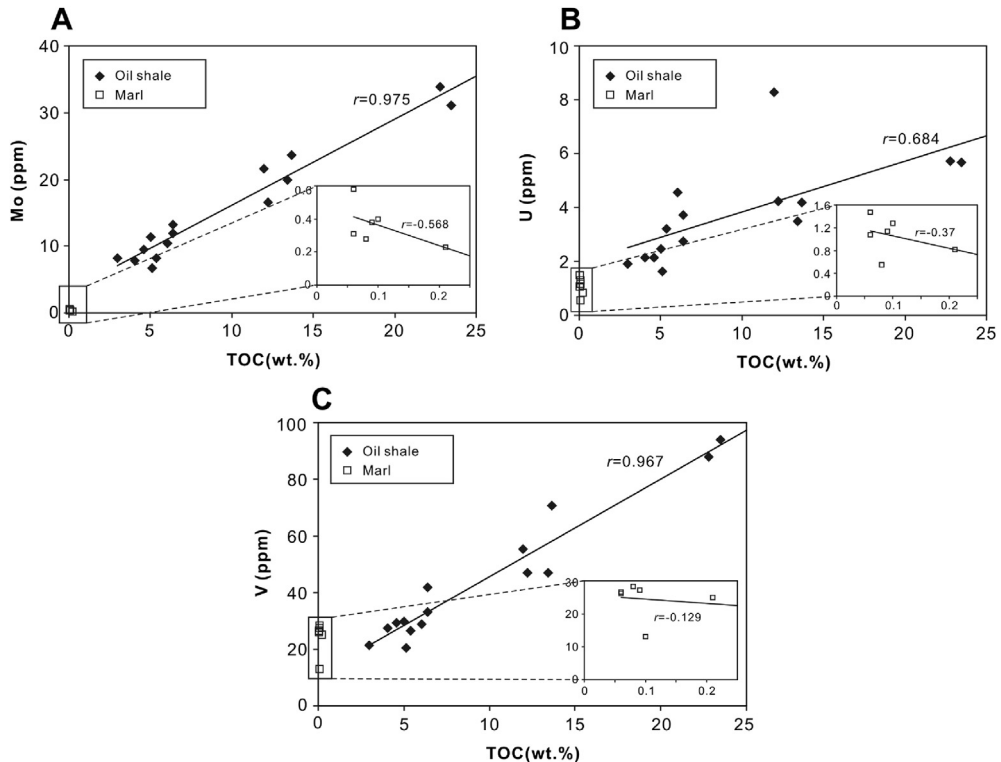


**Figure 12.** Crossplots of [Mo] (ppm), [U] (ppm) and [V] (ppm) versus total organic carbon (wt. %) of the samples in the Changliang Mountain oil shale profile, showing a good correlation of TOC and Mo, U and V contents of the oil shale samples and a negative correlation during the marls deposition.

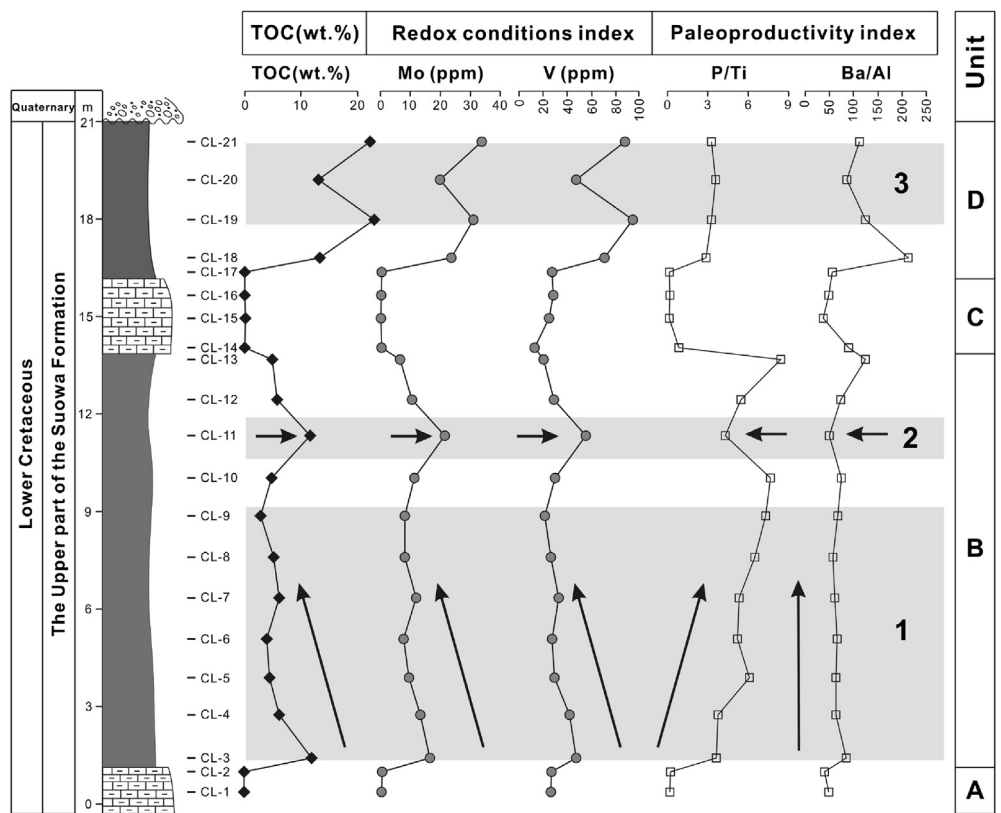


**Figure 13.** Stratigraphic distribution of TOC, P/Ti, Ba/Al, and Mo (redox condition and paleoproductivity proxies) in the Changliang Mountain oil shale section samples. The shadows are the three outstanding different variation sections of TOC, redox conditions index, and paleoproductivity index.

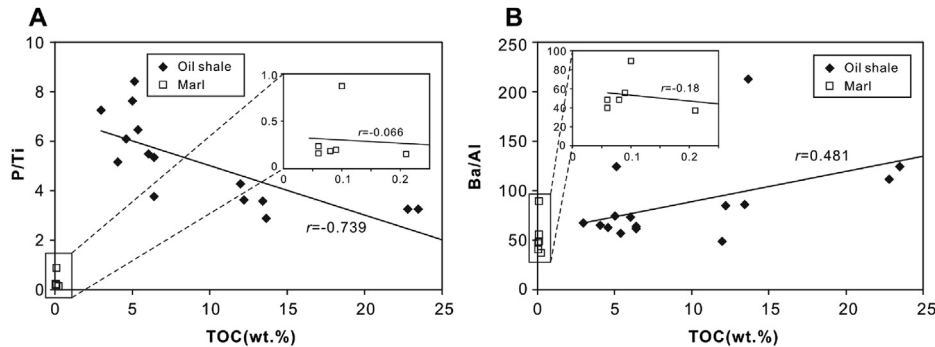


**Figure 14.** Relationship between (A) P/Ti, (B) Ba/Al and total organic carbon (TOC) in the Changliang Mountain oil shale profile, showing a negative or weak correlation between paleoproductivity and TOC contents. The solid line is the trend line for the parameters of all the samples.

sediments are lower. However, the vertical variation trend of the Ba/Al ratios is not well consistent with the content of TOC (Fig. 13). In Unit B, the TOC increase with depth, while the change of the Ba/Al ratio is not obvious excepting sample CL-13. In Unit D, the Ba/Al ratio of sample CL-18 reaches the highest value 213, while the content of TOC is 13.7%, which is nearly the same as sample CL-20 (13.4%), nevertheless, the Ba/Al ratio is 85.6 (Fig. 13). Besides, a weak correlation ( $r = 0.48$ ; Fig. 14) occurred between the Ba/Al ratios and TOC.

### 5.3. Controlling on the organic matter accumulation

Unlike most of the worldwide organic-rich oil shales deposited mainly in the fluctuating profundal facies of extensive deep or moderately deep lake environment (Liu, 2004; Zhu, 2009), the Changliang Mountain oil shale was deposited in lagoon environment (Wang et al., 2010a), whose deposition environment is similar to the Shengli River oil shale and Changshe Mountain oil shale in the North Qiangtang Basin (Fu et al., 2009b; Zeng et al., 2014). The accumulation of OM in marine sediments requires particular favorable conditions which are commonly considered to be related to: (i) high primary productivity (Sageman et al., 2003; Gallego-Torres et al., 2007; Wei et al., 2012; Fu et al., 2014); (ii) oxygen-deficiency in bottom waters (Canfield, 1989; Ingall et al., 1993; Arthur and Sageman, 1994; Mort et al., 2007); and (iii) a combination of both (Calvert and Fontugne, 2001; Rinna et al., 2002; Lézin et al., 2013).

As mentioned above, in the Changliang Mountain oil shale profile, several geochemical proxies indicate that all of the organic-rich sediments were deposited beneath a dysoxic to anoxic water column which is usually considered favorable for OM preservation. The weak or negative relationship between the productivity-related Ba/Al, P/Ti ratios and TOC contents ( $r = 0.418, -0.739$ , respectively; Fig. 14) and the good correlation between redox-related Mo, V and TOC contents ( $r = 0.98, 0.92$ , respectively; Fig. 12) suggest that accumulation of organic carbon mainly controlled by the dysoxic to anoxic conditions in the bottom water, which are beneficial to the OM enrichment. Although the oil shale Units B and D show a moderate to high primary productivity relative to the Ubara and the CCAL cores in Panthalassic Ocean (Algeo et al., 2011), the paleoproductivity proxies reveal different (or opposite) variation trend to the TOC contents (Fig. 13), which means that high primary productivity may not be the main factor for the organic rich oil shale formation. Therefore, a dysoxic to anoxic bottom water condition was the major controlling factor for OM accumulation during the Changliang Mountain oil shale deposition.

The  $w(\text{La})_N/w(\text{Yb})_N$  ratios (ratio of La and Yb normalized by the North American shale) are usually used to evaluate mudstone

sedimentary rate. If the sedimentary rate is fast, leading the rare earth element differentiation to be weakly, and the  $w(\text{La})_N/w(\text{Yb})_N$  value is close to 1 (Tenger et al., 2006). The  $w(\text{La})_N/w(\text{Yb})_N$  values of samples from the oil shale Units B and D in the Changliang Mountain area range from 1.18 to 1.45 and 1.22 to 1.37, with an average of 1.30 and 1.29, respectively, suggesting a fast sedimentary rate during the oil shale deposition, which would result in dilution of organic matter (Zhang et al., 2013).

As the Section 4.3.1 mentioned, elements Si, Ti, Zr, and Th concentrations data suggest high clastic fluxes derived from detrital aluminosilicate sources during the oil shale deposition. The increase in the clastic fluxes probably resulted from increased input of freshwater (Fu et al., 2014), which in turn could have rise to stratification of what has been interpreted as a paleo-lagoon (Fu et al., 2012). The stratification of the palaeo-lagoon water favored organic matter preservation (Bradley and Eugster, 1969; Desborough, 1978). As the above mentioned, the organic-rich oil shale in Units B and D formed in the similar redox condition and paleoproductivity, the different affects of freshwater input (Fig. 8B) maybe the main factor leading to the difference of TOC content between Units B and D.

The preservation of OM is a complex physical and chemical process, and several factors have been put forward as the primary controls on OM burial and preservation in sediments. Besides the primary productivity and redox factors, the mixed deposition with clay mineral also plays an important role during the preservation of OM. Kennedy et al. (2002) suggest that adsorption of carbon compounds onto clay mineral surfaces played a fundamental role in the burial and preservation of organic carbon. Clay-surface area may have provided physical protection to the OM (Ross and Bustin, 2009), enriching sediments with clay and organics (Jia et al., 2013). The elements Si, Al, and K are mainly associated with the clay minerals (Spears and Zheng, 1999). The positive correlations among these elements (Table 2) demonstrate that Si, Al, K and Ti mainly originate from a mixed clay assemblage, which is consistent with the occurrence of kaolinite, illite, and illite/smectite mixed layers. The positive relationship between K and Al ( $r = 0.99$ ) demonstrates that increases in Al are due to higher illite concentrations (the main host for K). The strong positive relationship between  $\text{K}_2\text{O}$ ,  $\text{Al}_2\text{O}_3$ ,  $\text{SiO}_2$  and TOC contents ( $r = 0.92, 0.92$ , and 0.89, respectively; Fig. 15) implies that clay minerals may influence OM preservation.

### 5.4. Formation model of the marine oil shale

Generally, the accumulation of significant volumes of organic-rich rock depends on the production and preservation of OM from aquatic and land plant, as well as on the clastic sedimentation rate (Huang et al., 2013). In the Qiangtang Basin, Fu et al. (2009) proposed that a prevalent contribution of algae to organic matter

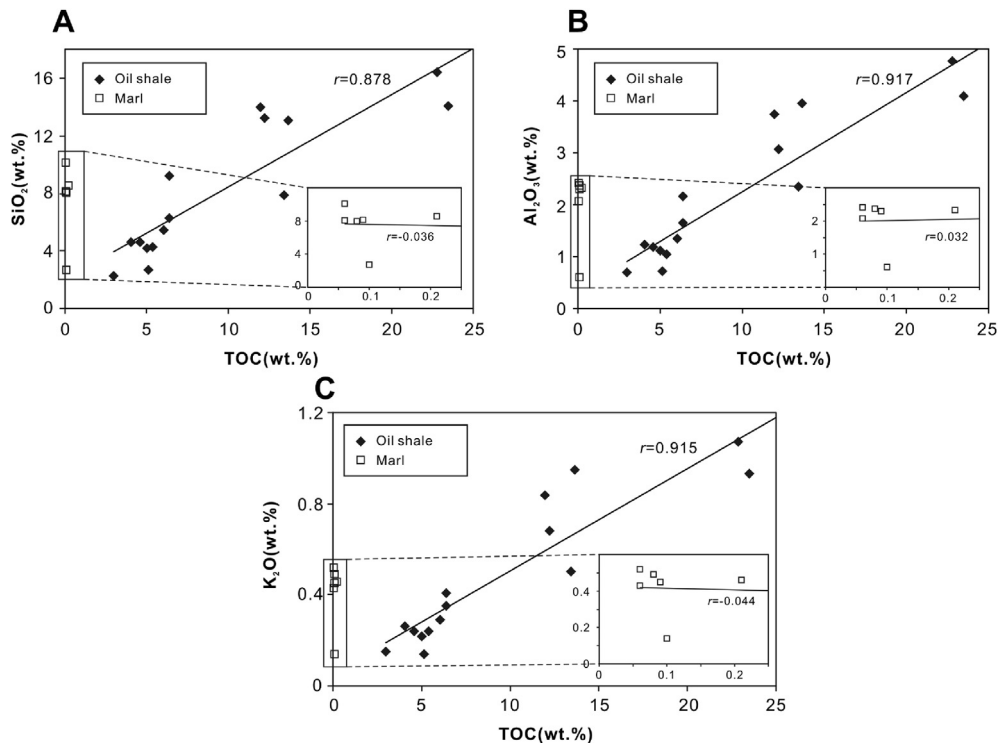


**Figure 15.** Crossplots of (A) SiO<sub>2</sub> (wt.%), (B) Al<sub>2</sub>O<sub>3</sub> (wt.%) and (C) K<sub>2</sub>O (wt.%) versus total organic carbon (TOC) (wt.%) of the samples in the Changliang Mountain oil shale profile, implying that clay minerals may influence OM preservation.

accumulation and the enrichment in <sup>13</sup>C is mainly attributing to the high productivity of algae in the Shengli River oil shale zone, which is within the same marine oil shale belt together with the Changliang Mountain oil shale. Therefore, the influence of the land plant on the accumulation of OM is very weak.

In the Changliang Mountain area, the marine organic-rich oil shale facies (Units B and D) was deposited in moderate to deep, oxygen-deficient, nutrient-rich, and stratified lagoon conditions, whereas the sedimentary environment during the marine marl facies (Units A and C) deposition was oxygenated shallow open marine environment, as demonstrated by the poor preservation of OM in the sediments.

The formation of the oil shale may approximately be divided into three major phases (Fig. 16) in the evolution of paleoenvironments during the Early Cretaceous in the Changliang Mountain region, North Qiangtang depression.

In the Qiangtang Basin, large-scale regressions could have taken place during the Early Cretaceous time (Wang et al., 2010a; Fu et al., 2009b), which gave rise to the formation of a barrier-lagoon system in the Changliang Mountain-Shengli River area (Fu et al., 2009b) when the relative sea level was low. Hence, the sediments in the Changliang Mountain area were mainly controlled by the Marguo Chaka uplift. At the beginning, the marl deposition (Unit A) is characterized by sedimentation in a well oxygenated shallow open marine environment while the relative sea level was high (Fig. 16A), as proved by the poor preservation of OM in the sediments, the abundant and diverse fauna (bivalves, brachiopods, pleopods, etc.) and microfaunal (foraminifer, calcareous nannofossils, etc.) assemblages, and the low values of paleoredox proxies in the marl sedimentary facies. According to the high Ti/Al and Si/Al ratios, it seems that the source of the detrital influx is probably nearby (Lézin et al., 2013). As Fu et al. (2009a) suggested, the climate of the Qiangtang Basin region was generally more hot and arid during the marl deposition period than that during the oil shale deposition

period on the basis of the variation in composition between oil shale and its overlying marl playnofloras. A hot and arid paleoclimate, combined with large and rapid influx, diluted the OM and killed the vegetation, which was unfavorable for the preservation of OM.

In the second phase, the Changliang Mountain area was isolated from the sea by Marguo Chaka uplift when the relative sea level dropped which was affected by regional tectonics (or global sea-level fluctuation) (Fig. 16B). An important paleoenvironment change is observed, marked by the OM enrichment during the oil shale deposition (Unit B). The initially dysoxic to anoxic conditions indicated by Mo, U, and Co enrichment probably lead to the disappearance of the benthic fauna (Fig. 17) and favor the preservation of OM in the sediments. During Unit B, a warm and humid or sub-humid environment prevails during the oil shale sedimentation. It is possible that, stratified, eutrophic, and nutrient-rich surface water may develop during such paleoclimate for the nutrients to have been periodically available to the microplankton, which could have produced episodes of basin eutrophication and algal blooms. A number of algal died and buried, and then caused most of the deposition of oil shales to be relatively dysoxic to anoxic (Chen et al., 2005), which can also be supported by abundant pyrite crystals found in oil shales (Fu et al., 2007) (Fig. 16B). The abundance of algal organic matter in these organic rich oil shales reflects an origin from the degradation of algal materials which were mostly preserved in the sediment record by sinking to the lagoon bottom where weak reduction bottom-water conditions existed.

During the deposition of Unit C, a better water-mass circulation was re-established in the Changliang Mountain area during this stage. The oxygen concentration gradually increases when the relative sea level rise, first of all leading to the occurrence of pelagic organisms (Fig. 16C), and then the appearance of benthic organisms and the disappearance of pyrites when oxygenation levels became sufficient in the sediments and water column (Fig. 16C). The

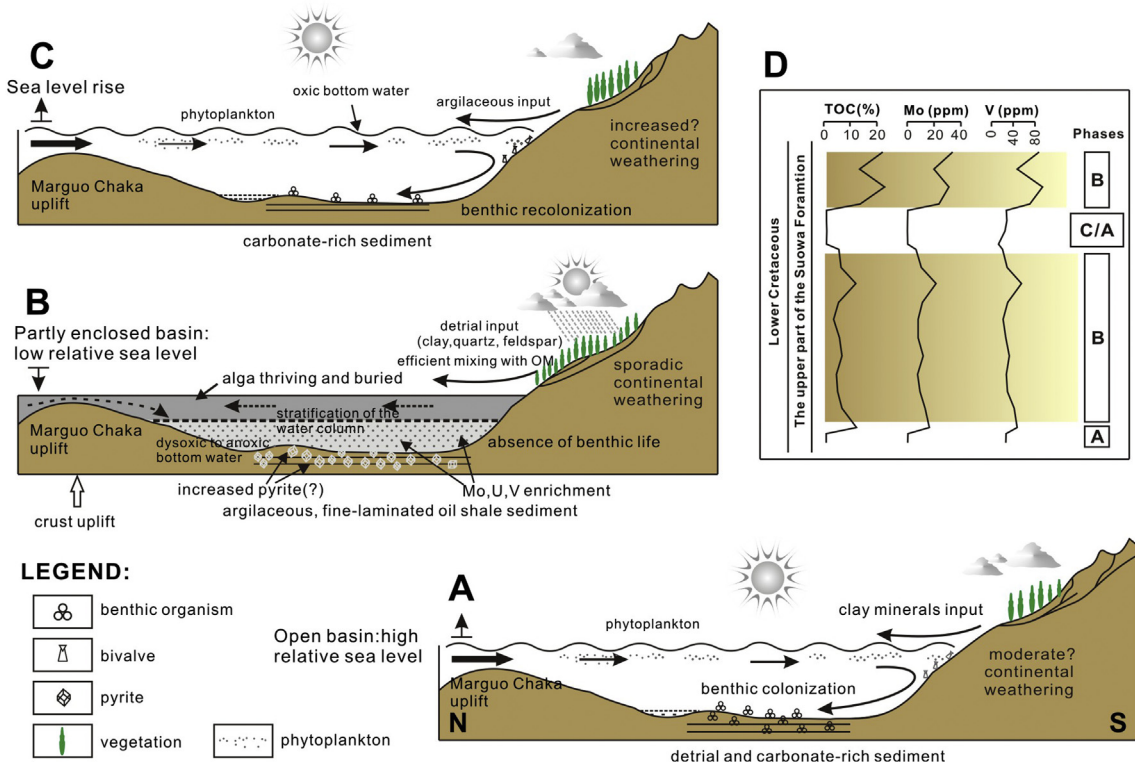


**Figure 16.** Diagrammatic sketch illustrating probable environment evolution during the Changliang Mountain oil shale-marl deposition in Qiangtang Basin (modified after Bour et al., 2007 and Lézin et al., 2013). (A) During the marl deposition (Unit A), a high relative sea level and a well oxygenated shallow open marine environment with high detrital influx occurred in the Changliang Mountain area under hot arid climate conditions favoring moderate degree continent weathering. (B) A low sea level occurred in the period of oil shale deposition (Unit B). This produced a partial enclosure of the basin, in which dysoxic to anoxic condition temporarily reach the base of the photic zone, associated with water-column stratification and Mo, U and V element enrichment. During this period, nannoplankton is scarce, benthic and bivalves are absent. Clay minerals along with freshwater input from the continent and an efficient mixing probably occur with the OM. In such water condition, a number of pyrites (?) were developed when the dysoxic to anoxic bottom water environment formed after the death and bury of the phytoplankton. (C) Water mass circulation re-established in the basin when sea level rises in Unit C, and oxic conditions reappear progressively along with pelagic and benthic fauna during the deposition of marl. (D) Inset showing the relative position of each phase with respect to TOC, Mo (ppm) and V (ppm) variations.

recovery of benthic and pelagic fauna reflects a normal marine environment (tide flat facies). As shown in Figure 13, paleoproductivity proxies (Ba/Al and P/Ti values) indicate a weak primary productivity. An oxic bottom water environment is confirmed by Mo/Al, V/Cr, Th/U, and Ni/Co values (Fig. 9). The

results indicate that changes in humidity related to sea level changes are responsible for the evolution of water salinity and redox conditions. The paleoclimate changed to be hot and arid during the deposition of marls, which was bad for the preservation of OM.

## 6. Conclusions

This reconstruction of the paleoenvironment and paleoproductivity conditions of the oil shales during Lower Cretaceous in Qiangtang Basin is mainly based on the study of geochemical analyses of the Changliang Mountain profile, combined with TOC contents, and a comparison with the paleoenvironment change recorded in other marine oil shale profiles in Qiangtang Basin.

- (1) The organic-rich oil shales (Units B and D) in the Changliang Mountain of the Qiangtang Basin contain from 2.96 to 23.47% TOC, while the TOC contents of marl (Units A and C) are generally low, ranging from 0.06 to 0.21%.
- (2) During the oil shale deposition (Units B and D), the Changliang Mountain area was isolated from the sea by Marguo Chaka uplift, along with the input of freshwater, leading to water stratification. Dysoxic/anoxic water conditions are widespread in the Changliang Mountain area, evidenced by the contents of redox-sensitive trace elements and their ratios. Subsequently, just after the oil shale deposition, normal oxygenation conditions gradually appear (Unit C), the



**Figure 17.** Bivalves-dominated benthic facies from the early-Cretaceous oil shale, northern Qiangtang Basin.

- bottom water environment changed to be well oxygenated, leading to the deposition of marls.
- (3) According to the paleoproductivity proxies, the primary productivity during the oil shale is moderate to high. However, the vertical variation trend of the paleoproductivity proxies is not well consistent with the content of TOC ( $r = 0.48$  and  $-0.74$ , respectively), indicating that primary productivity may not be the dominating factor controlling the preservation of OM.
- (4) A stratified water column and dysoxic to anoxic bottom water conditions are the major controlling factors of OM preservation during deposition of the Changliang Mountain oil shales, and a preservation model within the Changliang Mountain oil shale is established. In addition, factors such as mixed sedimentary with clay minerals, and detrital matter input cannot be ignored for their influence on OM enrichment.

## Acknowledgments

This work was supported by the National Natural Science Foundation of China (Nos. 41172098, 40972087), the National Oil and Gas Special Project (No. XQ-2009-01), and the Qiangtang Basin gashydrate resource exploration (No. GZH201400301). We thank Mr. Z. C. Yang and Mr. H. M. Luo for their logistical support in the field. Insightful suggestions and comments from Hui Tian and an anonymous reviewer, and Associate Editor Harish Veeramani are highly acknowledged.

## References

- Algeo, T.J., Maynard, J.B., 2004. Trace-element behavior and redox facies in core shales of Upper Pennsylvanian Kansas-type cycloths. *Chem. Geol.* 206, 289–318.
- Algeo, T.J., Ingall, E., 2007. Sedimentary Corg: P ratios, paleocean ventilation, and Phanerozoic atmospheric pO<sub>2</sub>. *Palaeogeogr. Palaeoclimatol. Palaeoecol.* 256, 130–155.
- Algeo, T.J., Kuwahara, K., Sano, H., Bates, S., Lyons, T., Elswick, E., Hinnov, L., Ellwood, B., Moser, J., Maynard, J.B., 2011. Spatial variation in sediment fluxes, redox conditions, and productivity in the Permian-Triassic Panthalassic Ocean. *Palaeogeogr. Palaeoclimatol. Palaeoecol.* 308, 65–83.
- Arthur, M.A., Sageman, B.B., 1994. Marine black shales: a review of depositional mechanisms and environments of ancient deposits. *Annu. Rev. Earth Planet. Sci.* 22, 499–552.
- Arthur, M.A., Dean, W.E., Laarkamp, K., 1998. Organic carbon accumulation and preservation in surface sediments on the Peru margin. *Chem. Geol.* 152, 273–286.
- Bradley, W.H., Eugster, H.P., 1969. Geochemistry and Paleolimnology of the Trona Deposits and Associated Authigenic Minerals of the Green River Formation of Wyoming: US Geological Survey Professional Paper 496-B, p. 71.
- Broecker, W.S., Peng, T.H., 1982. Tracers in the Sea. Eldigio Press, New York.
- Brumsack, H.-J., 2006. The trace metal content of recent organic-carbon-rich sediments: implications for Cretaceous black shale formation. *Palaeogeogr. Palaeoclimatol. Palaeoecol.* 232, 344–361.
- Bour, Y., Mattioli, E., Pittet, B., 2007. Nannofacies analysis as a tool to reconstruct paleoenvironmental changes during the Early Toarcian anoxic event. *Palaeogeogr. Palaeoclimatol. Palaeoecol.* 249, 58–79.
- Canfield, D.E., 1989. Reactive iron in marine sediments. *Geochim. Cosmochim. Acta* 53, 619–632.
- Canfield, D.E., 1994. Factors influencing organic carbon preservation in marine sediments. *Chem. Geol.* 114, 315–329.
- Calvert, S.E., 1987. Oceanographic controls on the accumulation of organic matter in marine sediments. In: Brooks, J., Fleet, A.J. (Eds.), *Marine Petroleum Source Rocks*. Blackwell, pp. 137–151.
- Calvert, S.E., Fontugne, M.R., 2001. On the Late Pleistocene–Holocene sapropel record of climatic and oceanographic variability in the eastern Mediterranean. *Paleoceanography* 16, 78–94.
- Calvert, S.E., Pedersen, T.F., 1993. Geochemistry of recent oxic and anoxic sediments: Implications for the geological record. *Mar. Geol.* 113, 67–88.
- Caplan, M.L., Bustin, R.M., 1998. Paleoceanographic controls on geochemical characteristics of organic-rich Exshaw mudrocks: role of enhanced primary productivity. *Org. Geochem.* 30, 161–188.
- Chen, L., Yi, H.S., Hu, R.Z., Zhong, H., Zou, Y.R., 2005. Organic geochemistry of the Early Jurassic oil shale from the Shuanghu area in northern Tibet and the Early Toarcian oceanic anoxic event (English Edition). *Acta Geol. Sin.* 79, 392–397.
- Crusius, J., Calvert, S., Pederson, T., Sage, D., 1996. Rhenium and molybdenum enrichments in sediments as indicators of oxic, sub-oxic and sulfidic conditions of deposition. *Earth Planet. Sci. Lett.* 145, 67–78.
- Dean, W.E., Gardner, J.V., Piper, D.Z., 1997. Inorganic geochemical indicators of glacial-interglacial changes in productivity and anoxia on the California continental margin. *Geochim. Cosmochim. Acta* 61, 4507–4518.
- Demaison, G.T., Moore, G.T., 1980. Anoxic environments and oil source bed genesis. *Org. Geochem.* 2, 9–31.
- Desborough, G.A., 1978. A biogenic-chemical stratified lake model for the origin of oil shale of the Green River Formation: an alternative to the playa-lake model. *Geol. Soc. Am. Bull.* 89, 961–971.
- Dymond, J., Suess, E., Lyle, M., 1992. Barium in deep-sea sediment: a geochemical proxy for paleoproductivity. *Paleoceanography* 7, 163–181.
- Dymond, J., Collier, R., 1996. Particulate barium fluxes and their relationships to biological productivity. *Deep-Sea Res. II* 43, 1283–1308.
- Dyni, J.R., 2006. Oil shale developments in the United States. *Oil Shale* 23, 97–98.
- DZ/T 0223-2001, 2001. *Geology Mineral Industry Standard of P.R. China: the General Analysis Rules for Inductively Coupled Plasma Mass Spectrometry (in Chinese)*.
- DZG 20.10-1990, 1990. *Geology Mineral Industry Standard of P.R. China: Rock and Mineral Analysis (in Chinese)*.
- Fedo, C.M., Young, G.M., Nesbitt, G.M., 1997. Paleoclimatic control on the composition of the Paleoproterozoic Serpent Formation, Huronian Super-group, Canada: a greenhouse to icehouse transition. *Precambrian Res.* 86, 201–223.
- Feng, L.J., Chu, X.L., Zhang, Q.R., Zhang, T.G., Li, H., Jiang, N., 2004. New evidence of deposition under a cold climate for the Xieshuuhe Formation of the Nanhua System in northwestern Hunan, China. *Chin. Sci. Bull.* 49, 1420–1427.
- Filippelli, G.M., Delaney, M.L., 1994. The oceanic phosphorus cycle and continental weathering during the Neogene. *Paleoceanography* 9, 643–652.
- Fu, X.G., Wang, J., Wang, Z.J., Chen, W.X., 2007. Marine oil shale depositional environment of Qiangtang Basin in northern Tibet. *Xinjiang Pet. Geol.* 28 (5), 529–533.
- Fu, X.G., Wang, J., Qu, W.J., Duan, T.Z., Du, A.D., Wang, Z.J., Liu, H., 2008. Re-Os (ICP-MS) dating of marine oil shale in the Qiangtang Basin, northern Tibet, China. *Oil Shale* 25 (1), 47–55.
- Fu, X.G., Wang, J., Zeng, Y.H., Li, Z.X., Wang, Z.J., 2009a. Geochemical and palynological investigation of the Shengli River marine oil shale (China): Implications for paleoenvironment and paleoclimate. *Int. J. Coal Geol.* 78, 217–224.
- Fu, X.G., Wang, J., Tan, F.W., Zeng, Y.H., 2009b. Sedimentological investigations of the Shengli River-Changshe Mountain oil shale (China): relationships with oil shale formation. *Oil Shale* 26 (3), 373–381.
- Fu, X.G., Wang, J., Zeng, Y.H., Tan, F.W., 2010a. REE geochemistry of marine oil shale from the Changshe Mountain area, northern Tibet, China. *Int. J. Coal Geol.* 81, 191–199.
- Fu, X.G., Wang, J., Tan, F.W., Chen, M., Chen, W.B., 2010b. The Late Triassic rift-related volcanic rocks from eastern Qiangtang, northern Tibet (China): age and tectonic implications. *Gondwana Res.* 17, 135–144.
- Fu, X.G., Wang, J., Zeng, Y.H., Tan, F.W., He, J.L., 2011. Geochemistry and origin of rare earth elements (REEs) in the Shengli River oil shale, northern Tibet, China. *Chem. Erde-Geochem.* 71, 21–30.
- Fu, X.G., Wang, J., Zeng, Y.H., Tan, F.W., Feng, X.L., 2012. Source regions and the sedimentary paleoenvironment of marine oil shale from the Bilong Co area, northern Tibet, China: An Sr-Nd isotopic study. *Oil Shale* 29, 306–321.
- Fu, X.G., Tan, F.W., Feng, X.L., Wang, D., Chen, W.B., Song, C.Y., Zeng, S.Q., 2014. Early Jurassic anoxic conditions and organic accumulation in the eastern Tethys. *Int. Geol. Rev.* 56 (12), 1450–1465.
- GB/T 19145-2003 (National Standard of P.R. China), 2003. *Determination of Total Organic Carbon in Sedimentary Rock (in Chinese)*.
- GB/T 215-2003 (National Standard of P.R. China), 2003. *Determination of Forms of Sulfur in Coal*. Standards Press of China, Beijing (in Chinese).
- Gallego-Torres, D., Martínez-Ruiz, F., Paytan, A., Jiménez-Espejo, F.J., Ortega-Huertas, M., 2007. Pliocene–Holocene evolution of depositional conditions in the eastern Mediterranean: role of anoxia vs. productivity at time of sapropel deposition. *Palaeogeogr. Palaeoclimatol. Palaeoecol.* 246, 424–439.
- Hatch, J.R., Leventhal, J.S., 1992. Relationship between inferred redox potential of the depositional environment and geochemistry of the Upper Pennsylvanian (Missourian) stark shale member of the Dennis limestone, Wabaunsee country, Kansas, USA. *Chem. Geol.* 99, 65–82.
- Helz, G.R., Miller, C.V., Charnock, J.M., Mosselman, J.F.W., PAttrick, R.A.D., Garner, C.D., Vaughan, D.J., 1996. Mechanism of molybdenum removal from the sea and its concentration in black shales: EFAXS evidence. *Geochim. Cosmochim. Acta* 60, 3631–3642.
- Holland, H.D., 1978. *The Chemistry of the Atmosphere and the Oceans*. Wiley-Interscience, New York.
- Huang, B.J., Tian, H., Wilkins, R.W.T., Xiao, X.M., Li, L., 2013. Geochemical characteristics, palaeoenvironment and formation model of Eocene organic-rich shales in the Beibuwan Basin, South China Sea. *Mar. Pet. Geol.* 48, 77–89.
- Ibach, L.E.J., 1982. Relationship between sedimentation rate and total organic carbon content in ancient marine sediments. *AAPG Bull.* 66, 170–188.

- Ingall, E.D., Bustin, R.M., Van Cappellen, P., 1993. Influence of water column anoxia on the burial and preservation of carbon and phosphorus in marine shales. *Geochim. Cosmochim. Acta* 57, 303–316.
- Jia, J.L., Bechtel, A., Liu, Z.J., Strobl, S.A.I., Sun, P.C., Sachsenhofer, R.F., 2013. Oil shale formation in the Upper Cretaceous Nenjiang Formation of the Songliao Basin (NE China): Implications from organic and inorganic geochemical analyses. *Int. J. Coal Geol.* 113, 11–26.
- Jones, B., Manning, D.A.C., 1994. Comparison of geochemical indices used for the interpretation of palaeoredox conditions in ancient mudstones. *Chem. Geol.* 111, 111–129.
- Kapp, P., Yin, A., Manning, C.E., Harrison, T.K., Taylor, M.H., Ding, L., 2003. Tectonic evolution of the early Mesozoic blueschist-bearing Qiangtang metamorphic belt, central Tibet. *Tectonics* 22, 10–43.
- Kennedy, M.J., Pevear, D.R., Hill, R.J., 2002. Mineral surface control of organic carbon in black shale. *Science* 295, 657–660.
- Kidder, D.L., Erwin, D.H., 2001. Secular distribution of biogenic silica through the Phanerozoic: comparison of Silica-replaced fossils and bedded cherts at the series level. *J. Geol.* 109, 509–522.
- Kimura, T., 1998. Relationships between inorganic elements and minerals in coals from the Ashibetsu district, Ishikari coal field, Japan. *Fuel Process. Technol.* 56, 1–19.
- Kimura, H., Watanabe, Y., 2001. Ocean anoxia at the Precambrian-Cambrian boundary. *Geology* 29, 995–998.
- Kök, M.V., 2006. Oil shale resources in Turkey. *Oil Shale* 23 (3), 209–210.
- Lash, G.G., Blood, D.R., 2014. Organic matter accumulation, redox, and diagenetic history of the Marcellus Formation, southwestern Pennsylvania, Appalachian basin. *Mar. Pet. Geol.* 57, 244–263.
- Lézin, C., Andreu, B., Pellenard, P., Bouchez, J.-L., Emmanuel, L., Fauré, P., Landrein, P., 2013. Geochemical disturbance and paleoenvironmental changes during the Early Toarcian in NW Europe. *Chem. Geol.* 341, 1–15.
- Liu, M.Q., 2004. The assumed gas accumulation systems in Beibuwan basin. *China Offshore Oil Gas* 16 (2), 93–97.
- Liu, Y., Liu, H.C., Li, X.H., 1996. Simultaneous precise determination of 40 trace elements in rock samples using ICP-MS. *Geochemica* 25 (6), 552–558.
- Liu, Z.J., Yang, H.L., Dong, Q.S., Zhu, J.W., Guo, W., Ye, S.Q., Liu, R., Meng, Q.T., Zhang, H.L., Gan, S.C., 2009a. Oil Shale in China. Petroleum Industry Press, Beijing, pp. 1157–1167.
- Liu, Z.J., Meng, Q.T., Liu, R., 2009b. Characteristics and genetic types of continental oil shales in China. *J. Paleogeogr.* 11 (1), 105–114.
- Luo, Q.Y., Zhong, N.N., Zhu, L., Wang, Y.N., Qin, J., Qi, L., Zhang, Y., Ma, Y., 2012. Correlation of burial organic carbon and paleoproductivity in the Meso-proterozoic Hongshuihuang Formation, northern North China. *Chin. Sci. Bull.* <http://dx.doi.org/10.1007/s11434-012-5534-z>.
- McLennan, S.M., 1993. Weathering and global denudation. *J. Geol.* 101, 295–303.
- Mort, H., Jacquat, O., Adatte, T., Steinmann, P., Föllmi, K., Matera, V., Berner, Z., Stüben, D., 2007. The Cenomanian/Turonian anoxic event at the Bonarelli Level in Italy and Spain: enhanced productivity and/or better preservation? *Cretac. Res.* 28, 597–612.
- Murphy, A.E., Sageman, B.B., Hollander, D.J., Lyons, T.W., Brett, C.E., 2000. Black shale deposition and faunal overturn in the Devonian Appalachian basin: clastic starvation, seasonal water-column mixing, and efficient biolimiting nutrient recycling. *Paleoceanography* 15, 280–291.
- Murray, R.W., Leinen, M., Isern, A.R., 1993. Biogenic flux of Al to sediment in the central equatorial Pacific Ocean: evidence for increased productivity during glacial episodes. *Paleoceanography* 8, 651–670.
- Murray, R.W., Leinen, M., 1996. Scavenged excess aluminum and its relationship to bulk titanium in biogenic sediment from the central equatorial Pacific Ocean. *Geochim. Cosmochim. Acta* 60, 3869–3878.
- Myers, K.J., Wignall, P.B., 1987. Understanding Jurassic organic-rich mud-rocks – new concepts using gamma ray spectrometry and palaeoecology: examples from the Kimmeridge clay of Dorset and the Jet rock of Yorkshire. In: Leggett, J.K., Zuffa, G.G. (Eds.), *Marine Clastic Sedimentology*. Graham and Trotman, London, pp. 1–45.
- Meyer, E.E., Burgeen, B.N., Lackey, H., Landis, J.D., Quicksall, A.N., Bostick, B.C., 2008. Evidence for basin restriction during syn-collisional basin formation in the Silurian Arisaig Group, Nova Scotia. *Chem. Geol.* 256, 1–11.
- Nesbitt, H.W., Young, G.M., 1982. Early Proterozoic climates and plate motions inferred from major element chemistry of lutesites. *Nature* 299, 715–717.
- Nesbitt, H.W., Young, G.M., 1989. Formation and diagenesis of weathering profiles. *J. Geol.* 97, 129–147.
- Nesbitt, H.W., Young, G.M., 1996. Petrogenesis of sediments in the absence of chemical weathering: effects of abrasion and sorting on bulk composition and mineralogy. *Sedimentology* 43, 341–358.
- Paytan, A., Kastner, M., Chavez, F.P., 1996. Glacial to interglacial fluctuations in productivity in the equatorial Pacific as indicated by marine barite. *Science* 274, 1355–1357.
- Paytan, A., Griffith, E.M., 2007. Marine barite: recorder of variations in ocean export productivity. *Deep-Sea Res. II* 54, 687–705.
- Pedersen, T.F., Calvert, S.E., 1990. Anoxia vs. productivity: what controls the formation of organic-carbon-rich sediments and sedimentary rocks? *AAPG Bull.* 74, 454–466.
- Piper, D.Z., 1994. Seawater as the source of minor elements in black shales, phosphorites, and other sedimentary deposits. *Chem. Geol.* 115, 95–114.
- Rimmer, S.M., 2004. Geochemical paleoredox indicators in Devonian-Mississippian black shales, central Appalachian Basin (U.S.A.). *Chem. Geol.* 206, 373–391.
- Rinna, J., Warning, B., Meyers, P.A., Brumsack, H.J., Bullkotter, J., 2002. Combined organic and inorganic geochemical reconstruction of paleodepositional conditions of a Pliocene sapropel from the eastern Mediterranean Sea. *Geochim. Cosmochim. Acta* 66, 1969–1986.
- Ross, D.J.K., Bustin, R.M., 2009. Investigating the use of sedimentary geochemical proxies for paleoenvironment interpretation of thermally mature organic-rich strata: examples from the Devonian–Mississippian shales, Western Canadian Sedimentary Basin. *Chem. Geol.* 260, 1–19.
- Sageman, B.B., Murphy, A.E., Werne, J.P., Ver Straeten, C.A., Hollander, D.J., Lyons, T.W., 2003. A tale of shales: the relative roles of production, decomposition, and dilution in the accumulation of organic-rich strata, Middle-Upper Devonian, Appalachian basin. *Chem. Geol.* 195, 229–273.
- Scott, C., Lyons, T.W., Bekker, A., Shen, Y., Poulton, S.W., Chu, X., Anbar, A.D., 2008. Tracing the stepwise oxygenation of the Proterozoic ocean. *Nature* 452, 456–459.
- Spears, D.A., Zheng, Y., 1999. Geochemistry and origin of elements in some UK coals. *Int. J. Coal Geol.* 38, 161–179.
- Sun, L.H., Gui, H.R., Chen, S., 2012. Geochemistry of sandstones from the Neo-proterozoic Shijia Formation, northern Anhui Province, China: Implications for provenance, weathering and tectonic setting. *Chem. Erde-Geochem.* 72 (3), 253–260.
- Tenger, Liu, W.H., Xu, Y.C., 2006. Comprehensive geochemical identification of highly evolved marine hydrocarbon source rocks: organic matter, paleoenvironment and development of effective hydrocarbon source rocks. *Chin. J. Geochim.* 25, 332–339.
- Tribouillard, N.-P., Desprairies, A., Lallier-Vergès, E., Bertrand, P., Moureau, N., Moureau, N., Ramdani, A., Ramanampisoa, L., 1994. Geochemical study of organic-matter rich cycles from the Kimmeridge clay formation of Yorkshire (UK): productivity versus anoxia. *Palaeogeogr. Palaeoclimatol. Palaeoecol.* 108, 165–181.
- Tribouillard, N., Algeo, T.W., Lyons, T., Riboulleau, A., 2006. Trace metals as paleoredox and paleoproductivity proxies: an update. *Chem. Geol.* 232, 12–32.
- Tyrrell, T., 1999. The relative influences of nitrogen and phosphorus on oceanic primary production. *Nature* 400, 525–531.
- Wang, J., Fu, X.G., Li, Z.X., Wu, T., He, J.L., 2009a. Discovery of the Shengli-Changsheshan oil shale belt in the Qiangtang basin, northern Tibet, China and its significance. *Geol. Bull. China* 28 (6), 691–695.
- Wang, J., Ding, J., Wang, C.S., Tan, F.W., Chen, M., Hu, P., Li, Y.L., Gao, R., Fang, H., Zhu, L.D., Li, Q.S., Zhang, M.H., Du, B.W., Fu, X.G., Li, Z.X., Wan, F., 2009b. Survey and Evaluation on Tibet Oil and Gas Resources. Geological Publishing House, Beijing.
- Wang, J., Fu, X.G., Li, Z.X., 2010a. Formation and significance of the oil shales from the north Qiangtang Basin. *Sediment. Geol. Tethyan Geol.* 30 (3), 11–17.
- Wang, J., Fu, X.G., Tan, F.W., Chen, M., He, J.L., 2010b. A new sedimentary model for the qiangtang Basin. *Acta Sedimentol. Sin.* 28, 884–893.
- Wang, P.J., Wang, D.P., Chang, P., Li, H., 1996. Metallic biomobilization of continental black shales. *J. Changchun Univ. Earth Sci.* 26, 47–53.
- Wang, C.S., Zhang, S.M., 1987. The discovery of oil shale in the Shuanghu area, Northern Tibet, China. *Geol. China* 8, 29–31.
- Wedepohl, K.H., 1971. Environmental influences on the chemical composition of shales and clays. In: Ahrens, L.H., Press, F., Runcorn, S.K., Urey, H.C. (Eds.), *Physics and Chemistry of the Earth*, vol. 8. Pergamon, Oxford, pp. 307–331.
- Wedepohl, K.H., 1991. The composition of the upper Earth's crust and the natural cycles of selected elements. Metals in natural raw materials. Natural resources. In: Merian, E. (Ed.), *Metals and Their Compounds in the Natural Environment*. VCH, Weinheim, Germany, pp. 3–17.
- Wei, H.Y., Chen, D.Z., Wang, J.G., Yu, H., Tucker, M.E., 2012. Organic accumulation in the lower Chihhsia Formation (Middle Permian) of South China: constraints from pyrite morphology and multiple geochemical proxies. *Palaeogeogr. Palaeoclimatol. Palaeoecol.* 353, 73–86.
- Wignall, P.B., 1994. *Black Shales*. Oxford University Press, New York.
- Wignall, P.B., Twitchett, R.J., 1996. Oceanic anoxia and the end Permian mass extinction. *Science* 272, 1155–1158.
- Wignall, P.B., Newton, R., 2001. Black shales on the basin margin: a model based on examples from the Upper Jurassic of the Boulonnais, northern France. *Sediment. Geol.* 144, 335–356.
- Yan, D.T., Chen, D.Z., Wang, Q.C., Wang, J.G., 2009. Geochemical changes across the Ordovician-Silurian transition on the Yangtze platform, South China. *Sci. China (Series D)* 52 (1), 38–54.
- Yan, D.T., Chen, D.Z., Wang, Q.C., Wang, J.G., 2010. Large-scale climate fluctuations in the latest Ordovician on the Yangtze block, south China. *Gology* 38 (7), 599–602.
- Yan, D.T., Wang, H., Fu, Q.L., Chen, Z.H., He, J., Zhan, G., 2015. Organic matter accumulation of Late Ordovician sediments in north Guizhou province, China: sulfur isotope and trace element evidences. *Mar. Pet. Geol.* 59, 348–358.
- Yin, A., Harrison, T.M., 2000. Geologic evolution of the Himalayan-Tibetan Orogen. *Annu. Rev. Earth Planet. Sci.* 28, 211–280.
- Young, G.M., Nesbitt, H.W., 1999. Paleoceanography and provenance of the glaciogenic Gowganda Formation (Paleoproterozoic), Ontario, Canada: a chemostratigraphic approach. *Geol. Soc. Am. Bull.* 111, 264–274.

- Zeng, S.Q., Wang, J., Chen, M., Fu, X.G., Wu, T., Xiong, X.G., 2012. Geological age, paleoclimate and petroleum geological characteristics of the upper part of the Suowa Formation in the North Qiangtang Basin. *Geoscience* 26 (1), 10–21.
- Zeng, S.Q., Wang, J., Fu, X.G., Feng, X.L., Chen, W.B., Sun, W., 2014. Characteristic and formation condition of the Cretaceous marine oil shale in the Qiangtang Basin. *Geol. Rev.* 60 (2), 449–463.
- Zhang, M.M., Liu, Z.J., Xu, S.C., Sun, P.C., Hu, X.F., 2013. Element response to the ancient lake information and its evolution history of argillaceous source rocks in the Lucaogou Formation in Sangonghe Area of Southern Margin of Junggar Basin. *J. Earth Sci.* 24, 987–996.
- Zhu, W.L., 2009. Paleolimnology and Source Rock Studies of Cenozoic Hydrocarbon-bearing, Offshore Basins in China. Geological Publishing House, Beijing, p. 297.